JOURNAL OF GEOPHYSICAL RESEARCH, VOL. 112, B04103, doi:10.1029/2005JB004028, 2007

Heterogeneous crust and upper mantle across southern Kenya and the relationship to surface deformation as inferred from magnetotelluric imaging

Max A. Meju[1] and Vassilis Sakkas[2]

Received 4 September 2005; revised 16 September 2006; accepted 21 November 2006; published 6 April 2007.

[1] We have used magnetotelluric data imaging to determine the resistivity structure across southern Kenya and our results suggest the presence of a buckled blocky or segmented lithosphere across the region. Prominent steep conductive zones at the Oloolollo (OLO) escarpment and eastern rift margin allow us to subdivide the region into three crustal domains. West of OLO, a bow-shaped conductor underlies a 10 km thick resistive upper crustal unit spatially correlating with an exposed Archaean greenstone belt. Between OLO and the eastern rift margin are found steeply dipping alternating conductive and resistive zones that appear buckled. East of this belt are found prominent, 5 to 20 km deep, subhorizontal conductors atop steep resistive blocks with flanking conductors. The main steep features in the crust appear to extend below the seismic Moho and thus suggest the presence of anomalously thick crust across the region. A 50 km-wide and 4–8 km deep w-shaped (double half-graben) structure is suggested at the position of the Kenyan rift. We show that our inferred lateral zoning is consistent with collocated gravity and seismic measurements. We propose a link between the deep resistivity heterogeneity and surface deformation pattern in the area.

Citation: Meju, M. A., and V. Sakkas (2007), Heterogeneous crust and upper mantle across southern Kenya and the relationship to surface deformation as inferred from magnetotelluric imaging, *J. Geophys. Res.*, *112*, B04103, doi:10.1029/2005JB004028.

1. Introduction

[2] The Proterozoic Mozambique orogenic belt (MOB) is part of the East African orogen [*Stern*, 1994] and exposes steep high-grade middle to lower crust widely believed to record the Neoproterozoic closure of an ocean basin which sutured east and west Gondwana [*Shackleton*, 1986, 1993, 1996; *Stern*, 1994]. Many linear Precambrian sutures and/or ophiolite belts are suggested to run N–S and NW–SE for several hundreds of kilometers from northeast Africa into the northern part of the MOB [*Berhe*, 1990] where they disappear under younger cover rocks (Figure 1). In southern Kenya and northern Tanzania (Figure 1), the MOB is bordered to the west by the Archaean Tanzania craton (West Gondwana). This region is also the locus of Cenozoic rifting and magmatism [e.g., *Bosworth*, 1987; *Smith*, 1994] such that much of the Precambrian terrain is covered by volcanic materials (Figure 1). Recent geophysical investigations have focused on understanding the lithospheric-scale structural controls on the rifting and magmatism [e.g., *Birt et al.*, 1997; *Byrne et al.*, 1997; *Tesha et al.*,1997; *Simpson*, 2000] and the extent of magmatic modification of the upper crust [*Simiyu and Keller*, 2001]. The precise relationship between the MOB and the Tanzania craton in this region is still not well understood and is central to our understanding of Precambrian tectonism [*Shackleton*, 1986, 1993, 1996; *Maboko*, 2000] and the link between Precambrian basement heterogeneity and Cenozoic rifting and magmatism in Kenya [e.g., *Bosworth*, 1987; *Mosley*, 1993; *Smith and Mosley*, 1993; *Birt et al.*, 1997]. Along the Kenya-Tanzania border (Figure 1), the craton exposes Archaean granitoid gneisses and metavolcanics while the MOB exposes mainly highly fractured quartzites and gneisses [*Simiyu and Keller*, 2001]. A 100-km-wide complex zone of ductile and brittle shears and thrust faults, bounded in the south by the Aswa-Nandi-Loita (ANL) shear zone and in the northeast by the Sekerr-Athi-Ikutha shear zone (Figure 1), is believed to place bounds on the respective craton and MOB margins [e.g., *Smith and Mosley*, 1993] but its deep structure is unknown and the Archaean basement-cover relation in the region has remained a subject of long-standing debate.

[3] *Shackleton* [1986] proposed an E-dipping suture zone at the western margin of the MOB in Kenya, exemplified by an outcropping 45^0 dipping zone of mylonitized Archaean rocks in thrust contact with Proterozoic metasediments and ophiolitic slivers to the east at Sekerr in northwestern Kenya (Figure 1). The suture zone is suggested to coincide with the Oloolollo escarpment (Figure 1) in southwest Kenya [*Shackleton*, 1986; *Tesha et al.*, 1997] and is supported by gravity studies near the Equator [e.g., *Nyblade and Pollack*, 1992; *Simiyu and Keller*, 1997]. However, some workers [*Smith*, 1994; *Birt et al.*, 1997] argue that the suture zone in

[1]Department of Environmental Science, Lancaster University, Lancaster, UK.
[2]Department of Geophysics, National and Kapodistrian University of Athens, Athens, Greece.

0148-0227/07/2005JB004028$09.00

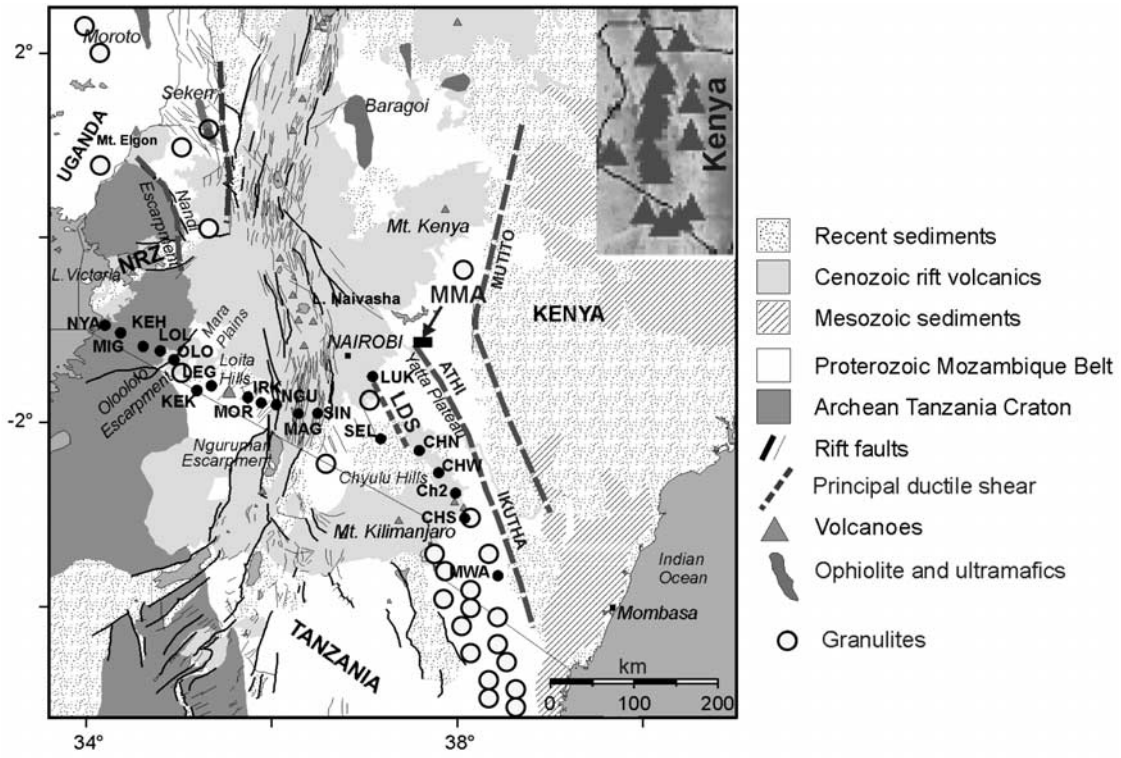

Figure 1. Geological map showing the locations of our collocated TEM and MT soundings in southern Kenya. The round dots show station positions. Station names are NYA (Nyamanga); MIG (Migori); KEH (Kehancha); LOL (Lolkorien); OLO (Ololoolo); KEK (Keekorok); LEG (Leganishu); MOR (Morijo); IRK (Irkiba); NGU (Nguruman); MAG (Magadi); SIN (Singleraine); LUK (Lukenya); SEL (Selengei); CHN (Chyulu north); CHW (Chyulu west); CH2 (Chyulu Range); CHS (Chyulu south); MWA (Mwatate). Principal basement structures from *Smith and Mosley* [1993]. NRZ, Nyanza rift zone. MMA, Matuu-Masinga area exposing Neoproterozoic arc granitoids [*Nyamai et al.*, 1999, 2003]. The distribution of granulites, ophiolites, and ultramafics in the region are also shown [*Shackleton*, 1986; *Smith and Mosley*, 1993]. Inset map highlights the known Holocene volcanoes in Kenya [*Bosworth*, 1987; *Smith*, 1994; *Macdonald*, 2003].

southern Kenya lies directly under the rift axis (and influenced rift evolution). Central to this argument is an area between Ololoolo and Magadi (Loita Hills in Figure 1) where Archaean crust is believed to be buried under gravitationally collapsed nappes and imbricated thrust slices of MOB rocks [*Mosley*, 1993; *Smith and Mosley*, 1993]. *Moller et al.* [1998] predict that a narrow zone of mixing of Archaean and Proterozoic crust extends from Tanzania to the Sekerr area and runs close to the craton in Kenya.

[4] Combined gravity and seismic refraction studies (KRISP94 Project) in southern Kenya [*Birt et al.*, 1997] suggest an essentially layered crustal structure across the region with the Moho depth varying from about 33 km in the Archaean craton to 40 km beneath the MOB east of the rift valley and did not show any sign of a suture at Ololoolo or crustal thrust zones (duplex-structures) in the Loita area. *Birt et al.* [1997] suggested that a low-density and low-velocity zone imaged in the upper mantle beneath the rift axis can be explained by the presence of up to 6% partial melt. The model of *Birt et al.* [1997] was used with wide-angle seismic reflection data to infer the existence of two discontinuous upper mantle reflectors (at depths varying between 43 and 63 km) extending beneath both flanks of the rift from the Ololoolo Escarpment, and ascribed to magmatic underplating [*Byrne et al.*, 1997, Figure 6]. *Simpson* [2000] suggests that long-period magnetotelluric (LMT) and magnetovariational (MV) data do not support the existence of partial melt in the upper mantle beneath the rift. On the basis of simple three-dimensional (3-D) forward modeling of limited MV and LMT data from stations MIG, OLO, KEK, LEG, MOR, IRK, NGU, MAG, SIN, and LUK in Figure 1, *Simpson* [2000] proposes the following: (1) The upper mantle is conductive to the west and resistive to the east of the western rift margin. (2) A crust of 1000 Ωm resistivity exists across the whole region. It is 80 km thick in the exposed Archaean craton west of the Ololoolo Escarpment and 40 km thick elsewhere. N–S trending, 3–5 km thick, conductive double half-grabens represent the Kenya Rift Valley, and two NW–SE-trending elongate conductive sheets (taken to represent 3-D middle/lower crustal lineaments) extend beneath both flanks of the rift from the Ololoolo Escarpment. However, it is unclear whether the predicted deep crustal lineaments and upper mantle divide actually relate to the outcropping NW–SE trending shear zones and Quaternary volcanoes in the region (see inset map in Figure 1) [*Bosworth*, 1987; *Smith*, 1994; *Macdonald*, 2003] previously suggested to influence long period MV data [e.g., *Banks and Beamish*, 1979].

[5] *Simiyu and Keller* [2001] provide a gravity model which incorporates deep seismic constraints [*Birt et al.*, 1997] and shows an E-dipping contact near the Oloolololo Escarpment in the top 15–18 km described as the crystalline upper crust. *Simiyu and Keller* [2001] also suggest that the low velocities and densities observed under the western flank of the rift probably represent reworked Archaean Tanzania craton. Thus the outstanding questions that have important tectonic implications in the region are (1) What are the precise extents of, and structural relationship between, the Archaean Tanzania craton and the MOB in southwestern Kenya? Is there a buried Archaean crust in the Loita area [*Mosley*, 1993]? (2) Is there an E-dipping suture zone near the Oloolololo Escarpment [*Shackleton*, 1986; *Simiyu and Keller*, 2001]? (3) How deep-rooted are the suggested Aswa-Nandi-Loita and Athi-Ikutha NW–SE lineaments seen on the surface? Do they extend vertically into the upper mantle or become listric and sole into a detachment surface possibly in the lower crust? Is there a link between basement heterogeneity and surface deformation or magmatism? (4) Is there partial melt in the mantle directly below the rift or a substantial disruption of the sub-Moho lithosphere in southern Kenya [*Birt et al.*, 1997; *Sakkas*, 1999; *Simpson*, 2000]? We believe that answers to these fundamental questions will enable us understand better any possible relationship between basement structure and Phanerozoic tectonism in the region [cf. *Smith and Mosley*, 1993; *Birt et al.*, 1997]. Also, any acceptable answers must be consistent with all the available geological and geophysical observations in the region.

[6] Two-dimensional (2-D) conductivity imaging of wide-bandwidth magnetotelluric (MT) data is successfully being used worldwide to study the regional structure and the distribution of fluids in steep fault-zones and orogenic belts [e.g., *Chen et al.*, 1996; *Ledo and Jones*, 2000; *Bai and Meju*, 2003; *Unsworth et al.*, 2004; *Soyer and Unsworth*, 2006]. Since the MOB of southern Kenya and northern Tanzania exposes steep middle to lower crust and large-scale shear zones [*Shackleton*, 1986, 1993; *Smith*, 1994; *Moller et al.*, 1998; *Maboko*, 2000], MT data imaging is appropriate for addressing the geological questions highlighted above. However, *Simpson* [2000] opines that there is no predominant or average regional geoelectrical strike direction across southern Kenya and that 2-D data imaging is therefore untenable. The available short-period MT data, shown elsewhere to be consistent with long-period data [*Simpson et al.*, 1997], were also deemed not to be of useable quality thus limiting the analysis to a subset [*Simpson*, 2000, Table 1] of the available MT data [*Sakkas*, 1999]. The NW–SE trending middle to lower crust lineaments that are central in Simpson's 3-D analysis are based on the suggested [*Smith and Mosley*, 1993] 100-km-wide zone of ductile shearing and thrusting that outcrops in the Athi area (Figure 1) and which should therefore provide some ground-truth for any workable model of the subsurface.

[7] There is no sign, in the upper crust of Simpson's resistivity model, of the prominent NW–SE basement structures seen on satellite imagery and identified on the surface [*Smith and Mosley*, 1993]. Given that where they cut the rift at the Equator, these NW–SE structures bound structural highs with depth to crystalline basement of <2 km [*Smith and Mosley*, 1993], is it possible that they are shallow-depth features? The KRISP94 line G seismic and gravity models [*Birt et al.*, 1997] suggest only minor modification of the shallow crust in the vicinity of the outcropping ductile shear zone near station CHN (feature labeled LDS in Figure 1). It will be instructive to examine the audiofrequency magnetotelluric (AMT) data along this particular seismic-gravity profile to ascertain any possible shallow-depth signature of the LDS and ANL shear zones and their relationship with the deep basement. A recent combined geological, geochemical and isotopic study identified a Neoproterozoic magmatic arc (see MMA in Figure 1) near the Athi-Ikutha shear zone [*Nyamai et al.*, 1999, 2003] raising the possibility of a concealed fossil subduction zone or hitherto unknown deep features in the region that can be imaged using the available LMT data. We posit that the reactivation of both shallow and deep systems of Precambrian shear zones and thrusts under varying stress conditions (possibly induced by lithospheric buckling) and their possible subsequent modification by fluids from the widespread Quaternary magmatism in this region should render them detectable by broadband MT conductivity imaging. There are therefore good grounds for re-analyzing all the available MT data, including our short period measurements [*Sakkas*, 1999], for the KRISP94 project with no a priori geological or geophysical assumptions and evaluating the result using independent information provided by other collocated geophysical measurements. This is the main thrust of the present paper and should enable us to better understand the resistivity structure of the region and its relevance to the on-going debate on craton-cover relations in southern Kenya and northern Tanzania.

2. Reanalysis of Broadband MT Data From Southern Kenya

[8] Collocated central- and single-loop transient electromagnetic (TEM) and wide-bandwidth (10^{-3} to 10^{4} s) MT data were recorded at stations spaced 10–20 km apart in southern Kenya close to the Kenya-Tanzania border (Figure 1) using two different field systems developed at Edinburgh and Gottingen Universities [*Simpson et al.*, 1997; *Sakkas*, 1999]. Although the first-order Proterozoic structures in Kenya trend NNW–SSE and N–S [*Smith and Mosley*, 1993], the survey orientation was dictated by accessibility and the seismic-gravity component of the integrated KRISP94 experiments [cf. *Birt et al.*, 1997; *Simpson et al.*, 1997]. The main 400 km long WNW–ESE MT survey line (KRISP94 Line G) consists of stations NYA to CHN in Figure 1 and runs from the Archaean Tanzania craton to the Quaternary volcanic field of Chyulu Hills, cutting across the Oloolololo Escarpment, the Loita Hills, Nguruman Escarpment, and the Kenya Rift Valley. The shorter LUK-MWA line (KRISP94 Line F) lies directly over a suggested lineament (herein conveniently called the Lukenya ductile shear zone, LDS in Figure 1). An L-shaped telluric configuration was used in our MT setup and formed the two corners of the 100 m-sided TEM transmitter loop, thus ensuring that both methods sampled the same geology. For each site, the AMT data were recorded in a day while LMT recordings were made over 10–14 days. The stations were mostly located on Cenozoic volcanic rocks with a few on Precambrian basement and alluvial outcrops (see Figure 1

Table 1. Summary of Distortion and Static Shift Analyses of the KRISP94 MT Data[a]

Stations	128–16 Hz	16–2 Hz	2 Hz to 4 s	4–32 s	40–1000 s	>1000 s	TE Shift Factor	TM Shift Factor	Local Geology
NYA	-	7	7	-	3		0.25	4.348	Nephelinites, granite
MIG	1	3	2	7	7	7	0.417	0.625	Rhyolites, granite
KEH	3	2	3	3	7	7	1	1	Shales, slates, slaty tuffs
LOL	-	2	3	7			7.143	5	Rhyolites, granite-greenstones
OLO	1	1	3	7	3		0.645	1.429	Phonolite, trachyte, olivine basalts
KEK	1	7	7	7	1		1	1	Quartzites
LEG	3	3	3	7	1		0.5	0.833	Quartzites
MOR	3	1	1	1	1		0.2	0.25	Quartzites/granite + alluvium
IRK	3	3	3	3	3		0.714	0.074	Quartzites + alluvium
NGU	1	1	1	7	3		0.526	1	Quartzofeldspathic gneiss
MAG	1	7	1	1	-	-	1.538	6.67	Trachyte and basalt
SIN	3	-	3	7	3	-	2	1.429	Trachyte and basalt
LUK	3	1	3	-	7	7	1	0.435	Mixed volcanics + tectonized granite
SEL	1	1	7	7	7	7	1	1	Marbles + olivine basalt, volcanic ash
CHN	7	7	7	7	7	-	1.667	0.377	Olivine basalt
CHW	-	-	2	7	3	-	5.55	55.55	Olivine basalt
CH2	1	-	7	7	-	-	5.55	6.25	Basalt, pyroclastics
CHS	7	1	-	-	3	-	0.667	2	Tectonized granite
MWA	1	1	7	7	7	7	1	9.09	Marbles

[a]Second to seventh columns show the classification of telluric distortions in the MT data (for six frequency bands) using the method of *Bahr* [1991]. Eighth and ninth columns give the multiplicative static shift factors determined using combined central- and single-loop TEM data for the two adopted MT data modes. Tenth column shows the local site geology. A dash in second to seventh column indicates a band for which no stable estimate was obtained.

and Table 1). One station located between SIN and SEL at the eastern rift flank was abandoned due to strong noise contamination of the MT records in that locality (Kajiado) and this severely affected our sampling density. The result for the LUK-MWA stations have been presented by *Sakkas et al.* [2002]. We are interested here in the NYA-CHN line. A subset of the long-period data for this line was used by *Simpson* [2000]. We will emphasize the short period data necessary for imaging the upper crustal structure across the poorly understood Loita area [*Mosley*, 1993; *Smith*, 1994] and the belt of exposed NW–SE shears at the eastern end of the transect. Note there is a 25 km offset between the starting points of the KRISP94 seismic and MT profiles referred to in this paper (our station NYA is at seismic position 25 km).

2.1. Regional Strike Determination and Near-Surface Static-Shift Correction With Multigeometry TEM Data

[9] All the KRISP94 MT field data [*Simpson et al.*, 1997; *Sakkas*, 1999] were reprocessed using tensorial analysis methods [*Groom and Bailey*, 1989; *Bahr*, 1991] and the result examined for dimensionality characteristics and static-shifts caused by near-surface heterogeneities. The result of initial analysis using the distortion classification method of *Bahr* [1991] is summarized in Table 1. It would appear from this table that the data for many sites show characteristics of weak local distortion (class 3) or fall into class 1 in the high frequency bands such that the tensor can be described using the conventional method. However, the data for a number of sites, particularly at the 4–32 s period band, appear to fall into class 7 with skew values greater than 0.3 suggesting a regional 3-D anomaly for which the superimposition model is not appropriate. Nevertheless, if the decomposition method yields a consistent regional strike for neighbouring stations, then the regional structure can be considered to be approximately 2-D [*Groom and Bailey*, 1989; *Bahr*, 1991]. It is significant that a detailed site-by-site examination of the distortion classes (Table 1) in relation to the quality of the unrotated apparent resistivity and phase data [see *Simpson*, 2000, Figure 2] revealed a strong correlation between those period bands that fall into class 7 and the noisiest MT (particularly phase) record segments. The same correlation also exists for our rotated data (shown later in Figure 3).

[10] The AMT induction arrows are of relatively poor quality when compared to long period data as also noted by *Simpson* [2000] and examples are shown in Figure 2a. However, three first-order observations can be drawn from Figure 2a. First, at high frequencies (>0.04 Hz), conductive boundaries are suggested between stations NYA and MIG (feature labeled F), near OLO (feature C), and at the western and eastern rift margins (features D and A, respectively). Feature C appears to be related to the surface-mapped craton-cover contact (CCC in Figure 2a) at high frequencies. The commonly assumed continental-scale lineaments (ANL and Athi-Ikutha shear zones) do not appear to influence the induction arrows at these frequencies. The LDS or another coincident but hitherto unknown feature appears to influence the induction arrows of the LUK-MWA stations at high frequencies. Second, at midfrequencies of about 0.04–0.014 Hz, the induction arrows suggest that feature C possibly exerts a major influence on the NYA-CHN line. It would appear that the ANL and Athi-Ikutha shear zones do not have a substantial influence on the NYA-CHN data while the LDS or another coincident regional conductor appears to influence the LUK-MWA sites at midfrequencies. Third, at low frequencies (<0.014 Hz), neither the ANL-LDS nor the Athi-Ikutha shear systems satisfactorily explain all the observed variations in amplitude and direction of the induction arrows. Rather, two deep conductive axes correlating with those suggested by *Banks and Beamish* [1979] and the trace of the Quaternary volcanoes appear to be regionally important. Significantly, one of these axes (labeled HVL in Figure 2a) coincides with an anomalous low-velocity zone inferred from 3-D teleseismic tomography to be well-developed at 23–70 km depth [*Ritter and Kasper*, 1997]. A general NW–SE trend is inferred for these possible conductive axes (Figure 2a).

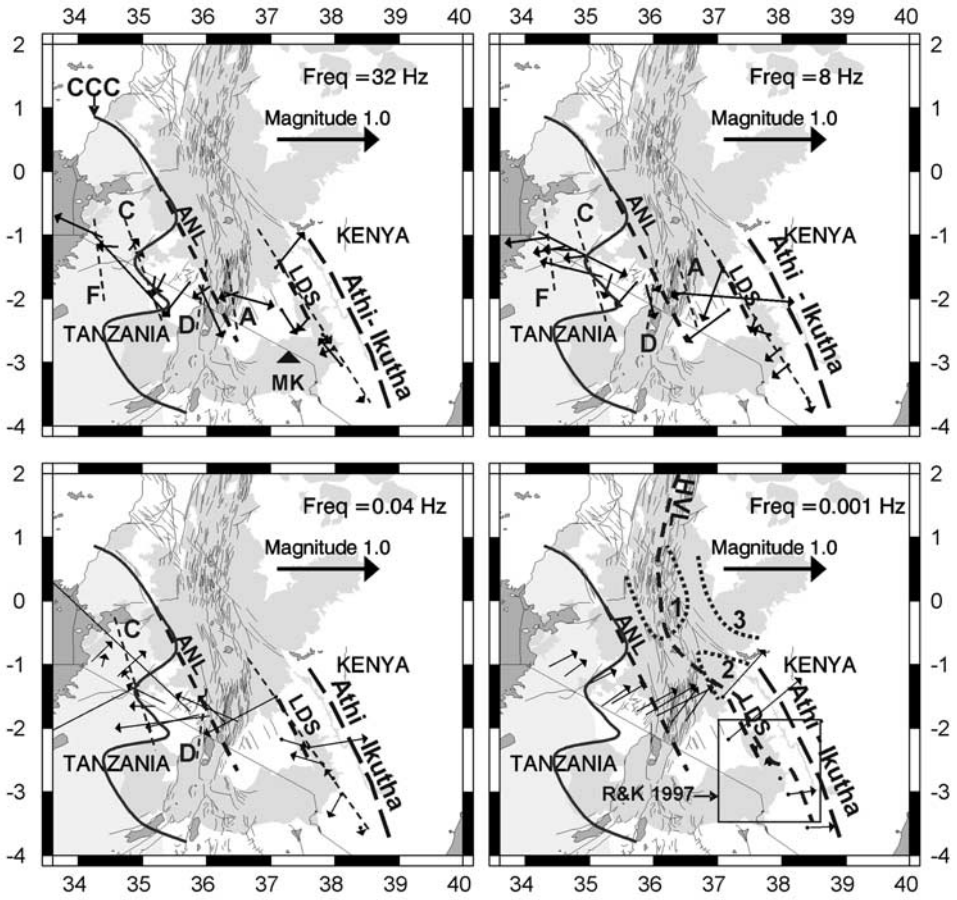

Figure 2a. Real Parkinson induction arrows for selected frequencies superimposed upon the regional geology map. CCC is the geologically mapped craton-cover contact on the surface. The possible areas of linear conductors that are consistent with the induction arrows are indicated by the dashed lines labeled "A," "C," "D," "F," and "HVL." In the lower right-hand panel, HVL (Holocene volcanic line) traces the position of major volcanic centres from the Chyulu Hills through Lake Naivasha to the north (see Figure 1) while the dotted lines numbered 1 to 3 denote the conductive zones mapped by *Banks and Beamish* [1979]. ANL (Aswa-Nandi-Loita shear zone) is a commonly assumed large-scale lineament.

[11] The unconstrained geoelectric strike directions computed from the MT impedance tensor [*Groom and Bailey*, 1989] are shown in Figure 2b Note that there is a 90 degrees ambiguity in the computed strike and other information must be used to select the correct direction. The azimuths for stations NYA to SEL on the main line show a dominant N23°–35°W (or N55°–67°E) trend especially at frequencies lower than 0.025 Hz. We take the NW–SE direction as the regional geoelectrical strike for the NYA-SEL segment since it agrees with the well-documented geological basement trend in the region [*Shackleton*, 1986; *Berhe*, 1990; *Smith and Mosley*, 1993] and the induction vectors (Figure 2a). The NE–SW azimuths computed for the LUK-MWA stations possibly suggest a high contrast boundary or a fundamental change in basement character at the eastern margin of the Kenya Rift; these stations lie close to outcropping NW–SE shear zones and a NW–SE trending low-velocity zone [*Ritter and Kasper*, 1997]. We found that mathematically rotating the impedance data for these stations by 90 degrees leads to strike angles that are consistent with those of the NYA-SEL segment. This is consistent with the natural behaviour of MT fields in the vicinity of a 2-D contact. There is therefore a consistent regional geoelectrical strike from these measurements but our WNW–ESE survey line runs somewhat oblique to it. It is noteworthy that 3-D teleseismic tomography clearly shows NW–SE-trending zones of anomalous velocity at 5–90 km depth in the Chyulu Hills area [*Ritter and Kasper*, 1997]. Also, nearer the Equator, *Rooney and Hutton* [1977] show a consistent electrical strike direction of N18°W along a WSW–ENE MT line across the rift (Figure 2b). A similar trend (see Figure 2a) is indicated by past long period MV studies in the region [*Beamish*, 1977; *Banks and Beamish*, 1979]. We noted that the unrotated data for stations IRK and LEG show phase splitting at high frequencies which possibly can be explained by the presence of 3-D elongate overburden sources [cf. *Sasaki and Meju*, 2006, Figure 5] but this will be difficult to constrain using the data from the widely spaced regional soundings. We consider that there are sufficient indications, from the above data analyses, that an approximate 2-D data imaging is valid for the NYA-CHN transect. The required transverse magnetic (TM) and transverse electric (TE) mode data for 2-D inversion were

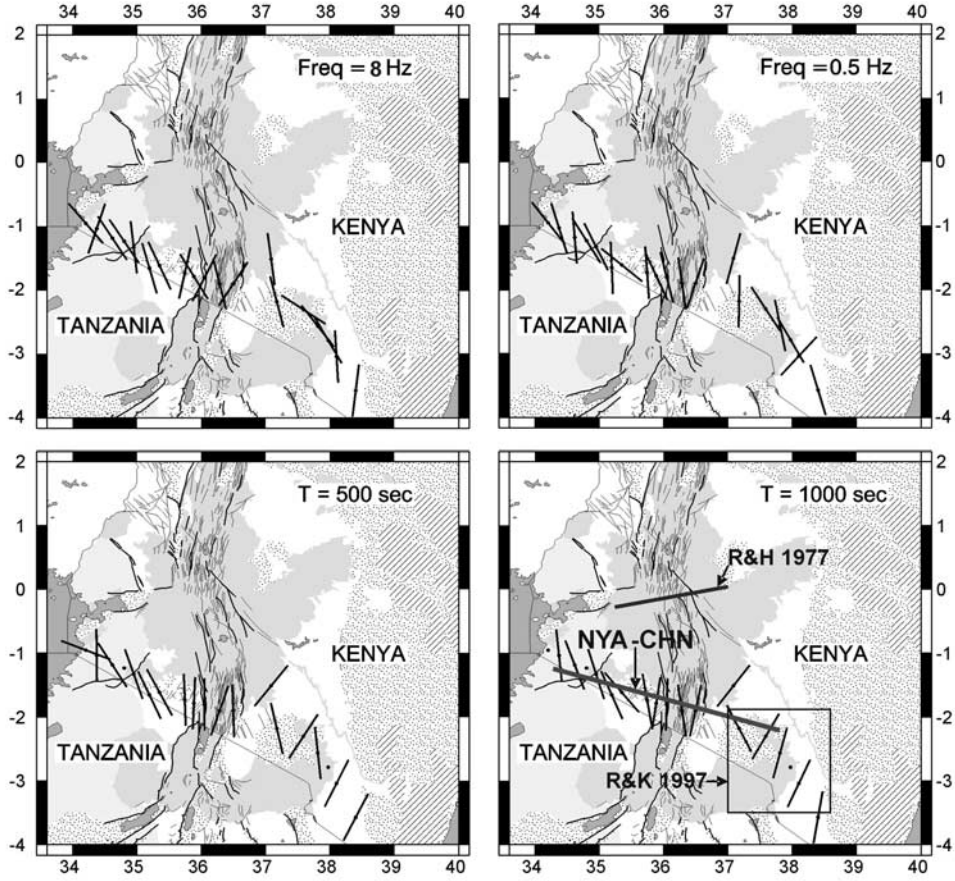

Figure 2b. Map showing the unconstrained *Groom and Bailey* [1989] azimuths of the MT impedance tensor at representative short and long periods sampling different depths. The data suggest a strong NW–SE basement structural trend from west to east along the NYA-CHN line. The thick solid line labeled R&H1977 shows the MT profile of *Rooney and Hutton* [1977]. The box labeled R&K1997 in Figures 2a and 2b shows the area where NW–SE trending lithospheric zones of alternating low and high velocities were imaged by three-dimensional (3-D) teleseismic tomography [*Ritter and Kasper*, 1997].

obtained by mathematically rotating the MT data into an adopted geoelectrical strike direction (N30°W).

[12] We then corrected all the dual-mode AMT and LMT apparent resistivity sounding curves for static-shift arising from near-surface heterogeneities using the dual-configuration TEM data [e.g., *Mohamed et al.*, 2002; *Sakkas et al.*, 2002; *Meju et al.*, 2003] as in the examples shown in Figure 3 (see Table 1 for all the correction factors), thus providing a stringent control of the level of MT apparent resistivities that is necessary for improved estimation of subsurface resistivity and interface depths. We recognize that this surface-consistent static-shift correction approach (weathering correction, sensu stricto) may not account for static-shift arising from deeper small-size 3-D heterogeneities [e.g., *Bahr et al.*, 2000]. However, it helps reduce the uncertainty in regional MT data interpretation and it has been demonstrated at several borehole sites that this approach leads to improved accuracy in depth mapping of geological formations [e.g., *Sternberg et al.*, 1988; *Meju*, 1996; *Meju et al.*, 1999]. Note that the sounding curve segments in Figure 3 that correspond to the 4–32 s period band falling into *Bahr*'s [1991] class 7 are characterized by poor signal levels (cf. OLO, NGU, and SIN in Table 1) while for other short-period bands it correlates to a frequency-dependent noisy segment (see the 2–5 Hz noise contamination at MAG in Figure 3). Such data segments will therefore be removed or down-weighted in our adopted 2-D inversion approach thus effectively removing the need for modelling what could be an unnecessary level of complexity in our data.

2.2. Qualitative Consistency Analysis of AMT and LMT Response Patterns

[13] As a qualitative check of the static-shift-corrected MT apparent resistivities across the Oloolo Escarpment and the Rift Valley, we show the adopted TE and TM mode data for selected short periods (32, 8, 0.5, 0.04 Hz) and long periods (500 and 1000 s) in Figure 4. The short period data are remarkably similar for both modes possibly suggesting relatively simple shallow crustal structures. There are no LMT data for station LOL west of OLO. Also, the TM mode LMT data at station SEL are of poor quality. Nevertheless, note the consistency in the pattern of variation of both the AMT and LMT apparent resistivities with distance. We therefore consider the AMT data to be of useable quality. Both the AMT and LMT data suggest strong lateral

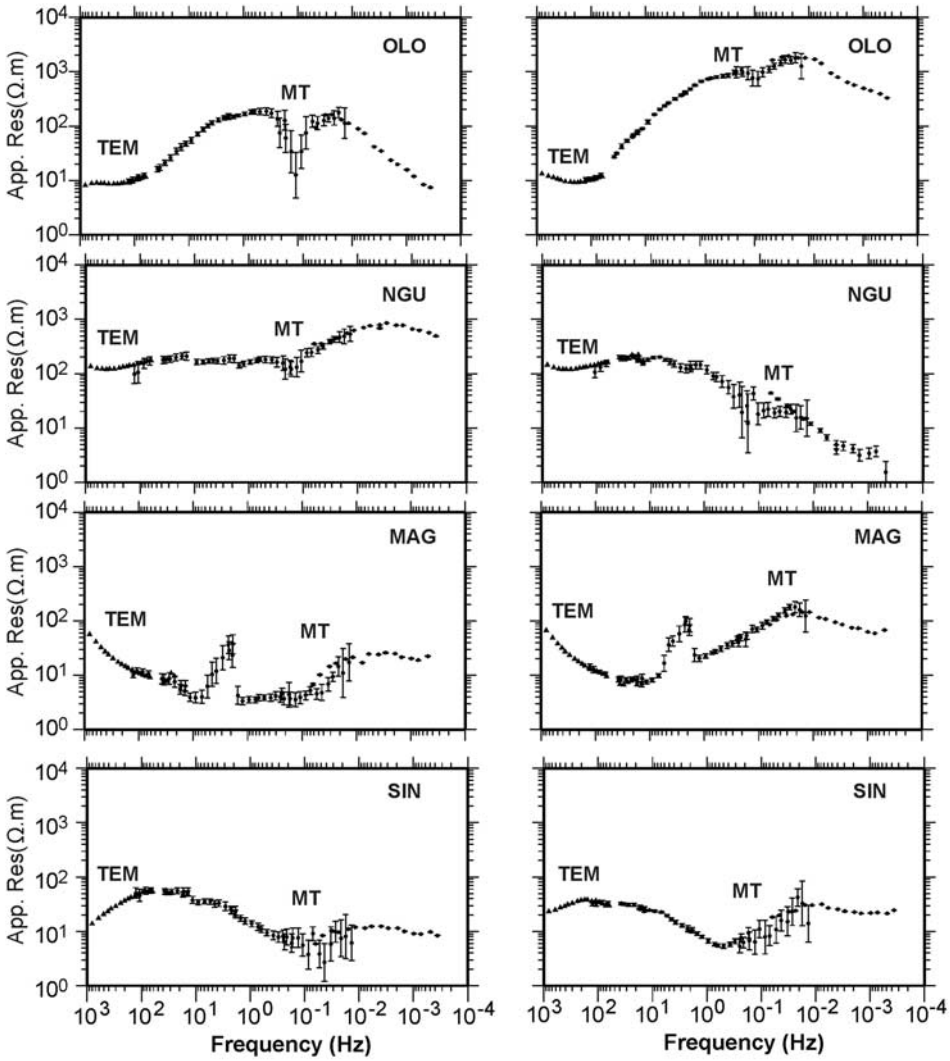

Figure 3. Illustration of MT data quality variations and method of dual-mode static-shift correction using multigeometry TEM data. For each station, the apparent resistivity data (shown with error bars representing 1 standard deviation) for the TE mode (left) and TM mode (right) are corrected using data from different TEM loop configurations that respond differently to lateral resistivity changes in the near-surface [e.g., *Sakkas et al.*, 2002]. Note the band-limited noisy segments of these frequency sounding curves (cf. Table 1).

changes at positions 70–90 km (spatially correlating with the OLO area) and near positions 200 and 250 km (spatially correlating with the western and eastern rift margins) as would be expected from theory for steep conductive contacts. The zone of high resistivity west of OLO coincides with an Archaean greenstone belt, that found between OLO and position 200 km correlates spatially with the Mara Plains and Loita Hills area where Archaean crust is thought to be deeply buried [*Mosley*, 1993], while that east of the main rift correlates with the Mozambique belt. There is thus good correlation between the apparent resistivity response and the known principal physiographic units on the NYA-CHN transect. This is taken as providing further support for the adopted 2-D data imaging approach described below. Exploring further the data selected for 2-D imaging, the impedance phases (shown later in Figure 6) at the eastern end of the profile (stations SEL and CHN) are less than 45° at the longest periods and the apparent resistivities rise in value suggesting that the crust or upper mantle at some depth there should be relatively resistive. Inside and west of the rift, the phases are consistently greater than 45° at periods longer than 100 s and suggest that a major basal conductor exists here at some depth.

3. Two-Dimensional Resistivity Imaging and Model Appraisal

3.1. Two-Dimensional Smooth Minimum-Structure Versus Structured Blocky Imaging

[14] An important consideration in this study is the fact that the exposed Precambrian basement in our study area is dominated by steep geological structures [*Shackleton*, 1986; *Smith and Mosley*, 1993]. It is well known that the TM mode data alone will not image narrow steep conductors

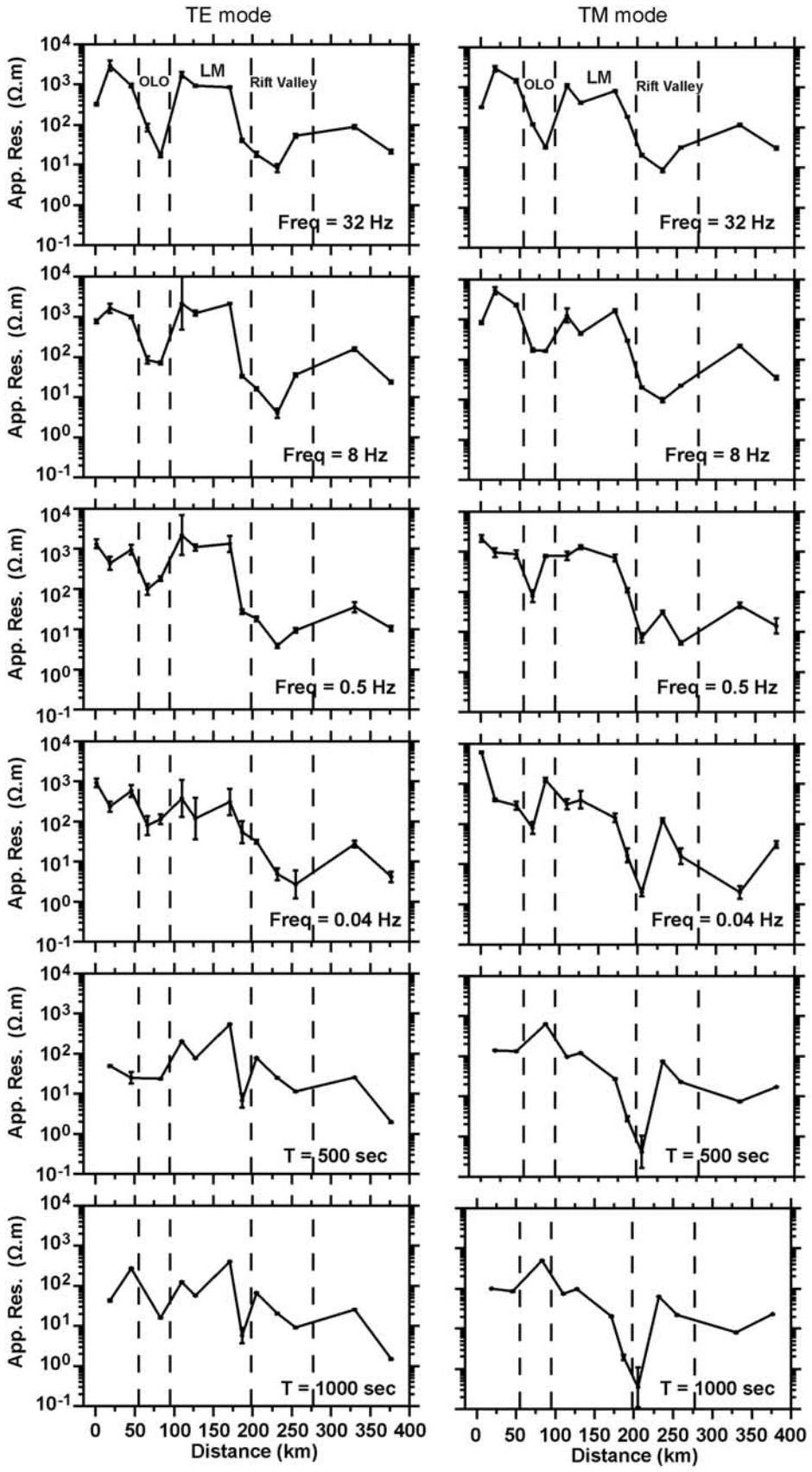
TE mode
TM mode
App. Res. (Ω.m)
OLO
LM
Rift Valley
Freq = 32 Hz
Freq = 8 Hz
Freq = 0.5 Hz
Freq = 0.04 Hz
T = 500 sec
T = 1000 sec
Distance (km)

Figure 4

and may overestimate the amount of conductive targets in the subsurface while the TE mode data, although more sensitive to narrow steep conductors and to the depth of buried conductive targets [e.g., *Wannamaker et al.*, 1984; *Agarwal et al.*, 1993], will be insufficient for characterizing the subsurface in 2-D. We therefore opted for joint imaging of the TE and TM mode apparent resistivity and phase data and especially since the short period data for both modes appear to be comparable (see Figure 4). The vertical magnetic field data (Figure 2a) were not considered for joint inversion with these MT responses since the induction arrows have relatively large errors at many sites especially at short periods [*Sakkas*, 1999]. An effective way of interpreting a sparse set of MT data is to seek the minimum number of parameters that can explain the data [*Constable et al.*, 1987]. We therefore experimented with reconstructing smooth models and follow-up structured (blocky) models to test how well our field data constrain the resistivity results. We used a regularized conjugate gradients inversion scheme for the minimum-structure imaging and a Gauss-Newton algorithm [*Mackie et al.*, 1997; *Rodi and Mackie*, 2001] for block-model imaging. Both algorithms allow the incorporation of surface topography, which we determined using differential GPS measurements (furnished by *Birt et al.* [1997]) and digital elevation models.

[15] In the minimum-structure inversion experiments, the emphasis was on reducing model-driven bias in the image reconstruction by using several half-space initial models of different resistivities (including 1000 Ωm used as background resistivity in the work of *Simpson* [2000]) and seeking the smoothest models that match our data. The average apparent resistivity for the data to be inverted was 794 Ωm for the AMT and 257 Ωm for the LMT data set (but 100 Ωm and 60 Ωm for IRK-CHN in the rift valley subregion). We therefore selected initial models of 50, 100, 200, 350, 500, and 1000 Ωm for our investigation and only those reconstructed structural features that are common to all the minimum-structure models may be considered necessary to fit the observed data. In all cases, the joint inversion was done with error thresholds of 5–10 percent (±10% for apparent resistivity and 5% for phase) set for the data, the same grid size (107 columns × 56 rows), a regularization or smoothing factor (τ) of between 5 and 10, and a normalized root-mean square (NRMS) error [*Rodi and Mackie*, 2001] of 1.5 as the threshold misfit. The smoothing was also allowed to vary with depth in different ways during the inversion exercise (not presented here) but appears not to lead to major structural differences in the top 40 km of the final models initiated with 50 to 350 Ωm and 500 to 1000 Ωm half-spaces especially west of the rift valley where there is good data coverage. Examples of 2-D imaging results for the 100 and 1000 Ωm half-spaces are shown in Figure 5a and 5b for the NYA-CHN transect. Both models equally match our field data. The fit between the field data and the computed responses of the model reconstructed from the 1000 Ωm half-space is shown in Figures 6a and 6b and has an NRMS error of 1.5 for the 2862 (TE and TM mode) data points inverted. The TE mode LMT data at MOR and OLO are poorly fitted and so are the data for KEK which we down-weighted in the inversion (by multiplying their standard errors by 2.2) for the reasons stated earlier. The fit between the field data and the computed responses for the 100 Ωm is only slightly poorer (NRMS error of 1.53) than that shown in Figures 6a and 6b. There are some structural differences between both models illustrating the nonuniqueness of the MT inverse problem and extraneous information must therefore be used to select the most likely model features. The common conductive structures in both models are labeled A to H but note that their absolute resistivity values are different. It is desirable to test whether the field data fully constrain these conductive features and the intervening resistive blocks using a blocky model and reliable external information.

[16] For the blocky model study, we constructed the top 20 km of our starting model using pieced-together results of 1-D joint inversion [*Meju*, 1996] of the rotationally invariant AMT and central-loop TEM data, assuming a near-layered crust as suggested by the available seismic velocity model [*Birt et al.*, 1997]. Below this 20 km crustal section, we drew on the 2-D images of Figure 5a and 5b from 20 to 48 km depth but made features C and D to be resistive and their flanking regions conductive. Below 48 km depth, we assigned a high resistivity (1000 Ωm) to the blocks located west of station SEL suggested to be conductive in the smooth models (Figures 5a and 5b) and low resistivity (20 Ωm) to areas eastward from SEL suggested to be resistive in the smooth models and also based on the qualitative analysis of LMT data presented above. Note that this is equivalent to adopting bad initial model parameters for sub-Moho depths and may lead to an unrealistic result. The grid size (107 columns × 56 rows) was kept the same for the several model runs testing different damping factors. The optimal least squares model resulting from this exercise is shown in Figure 5c. The model has an NRMS error of 1.74 for the 2862 data points inverted. Although the fit is poorer, the main resistivity features in the top 20 km (as well as deeper features near stations SEL and CHN) in this blocky model are comparable to those of the smooth models suggesting good data constraints on these features. However, the blocky model only marginally shows the possible presence of feature C east of OLO at greater than 20 km depth (cf. Figure 5a and 5c). An anomalous vertical conductor is suggested directly beneath OLO at 48 km depth while an E-dipping conductor appears to connect from the near-surface at NGU to another conductive zone (feature E) at 48 km depth below the western rift margin. The resistive blocks in the Loita and SEL areas seem to extend beyond 100 km depth in the blocky model. It would thus appear that the lateral extents of both the resistive and conductive blocks at subcrustal depths are not well-constrained by the present data and/or that the initial blocky model was unrealistic. It is also obvious from this comparative study that a near-horizontally layered structure may be inappropriate for at least the top 20 km of the crust west of

Figure 4. Variation of static-shift corrected dual-mode MT apparent resistivities with distance. Shown are representative AMT (32, 8, 0.5, and 0.04 Hz) and LMT (500 and 1000 s) data profiles from the two different MT field equipment deployed in the KRISP94 study. Left panels show TE mode; right panels show TM mode. The vertical dashed lines indicate the Oloolo area (OLO), the Loita Hills and Mara Plains sector (LM) and the Kenya Rift Valley.

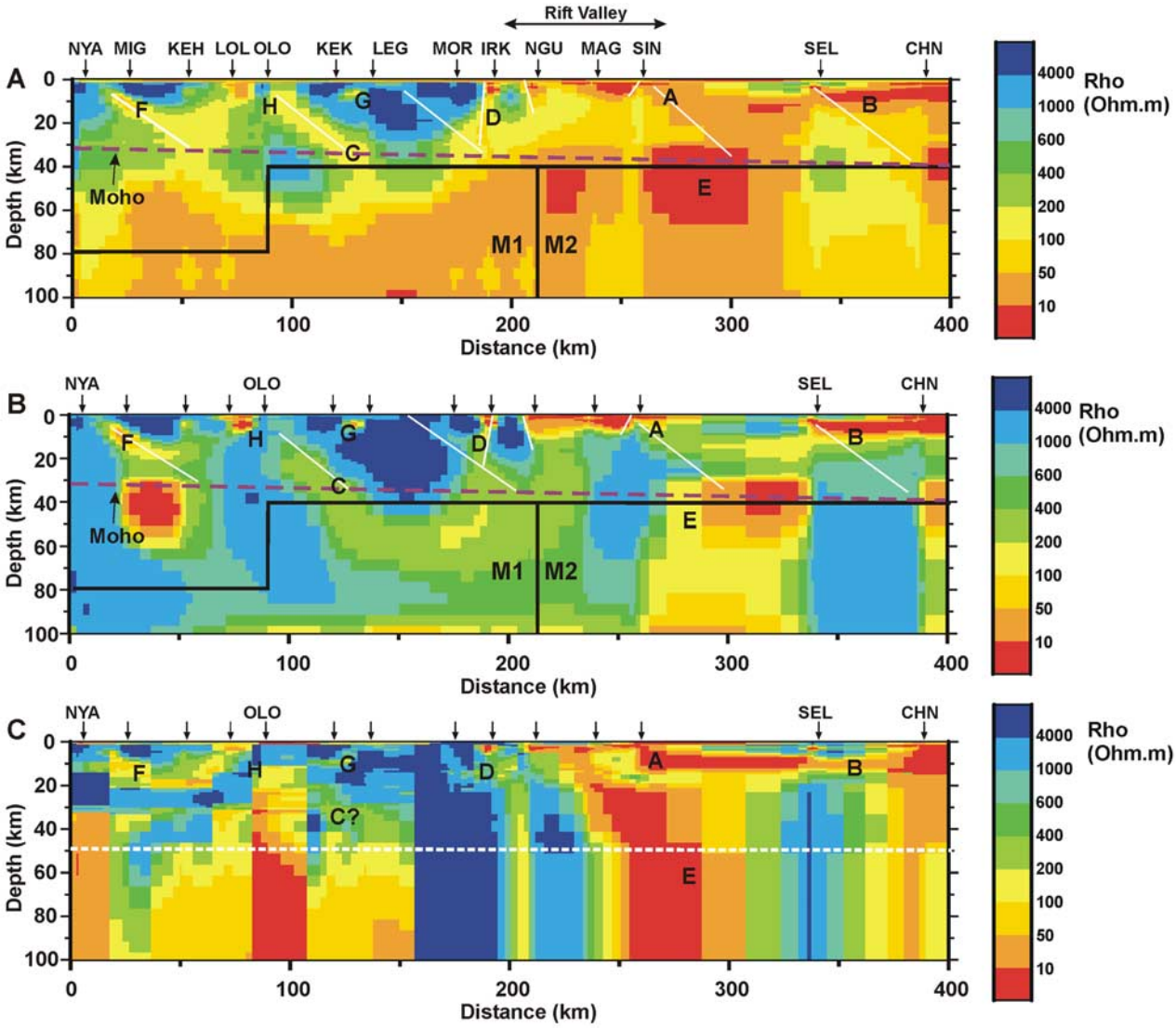

Figure 5. Comparison of statistically equivalent results of 2-D smoothness-constrained resistivity inversion and a blocky model constructed using a purposely designed poor initial model to test data constraint on upper mantle structures. The smoothness-constrained models were generated using initial half-space resistivities of (a) 100 Ωm and (b) 1000 Ωm. In Figures 5a and 5b, the purple dashed line represents the seismic Moho [*Birt et al.*, 1997] while the thin white lines above it indicate possible parallelism of the steep E-dipping segments of prominent conductive features. *Simpson*'s [2000] proposed structure of the upper mantle (conductive in the west, M1; resistive in the east, M2) is indicated by the thick black lines in both models. The blocky 2-D inversion model is shown in Figure 5c and the white horizontal dashed line at 48 km depth marks the top of the alternating conductive and resistive blocks used in the starting model to test data constraint on upper mantle features. The conductive features labeled A to G are common to all the models and are described in text. The MT sounding points are denoted by arrows at the top of each panel. Hot colors (yellow and red) indicate high conductivity and cool colors (blue and purple) indicate high resistivity. No vertical exaggeration.

the main rift. Before any geological inference can be drawn from the above resistivity models, it is important to ascertain further that all the suggested common crustal features are statistically robust and satisfy other available geophysical data.

3.2. Simplest Quantitative Model Appraisal

[17] The blocky model shown in Figure 5c was selected for appraisal since it contains more features than the minimum-structure models which could be due to overinterpretation of the finite set of field data. Assuming an average error level of 10 percent in our field data (cf. Figures 6a and 6b) and the model of Figure 5c as the optimal regularized inversion model ($\mathbf{m}_{\mathrm{nrms}}$) with a normalized residual error $\mathbf{Q}_{\mathrm{nrms}}$, we sought the range of model parameters that will yield a threshold misfit ($\mathbf{Q}_{\mathrm{t}}$) given by

$$\mathbf{Q}_{\mathrm{t}} = \mathbf{Q}_{\mathrm{nrms}} \times 1.1 \qquad (1)$$

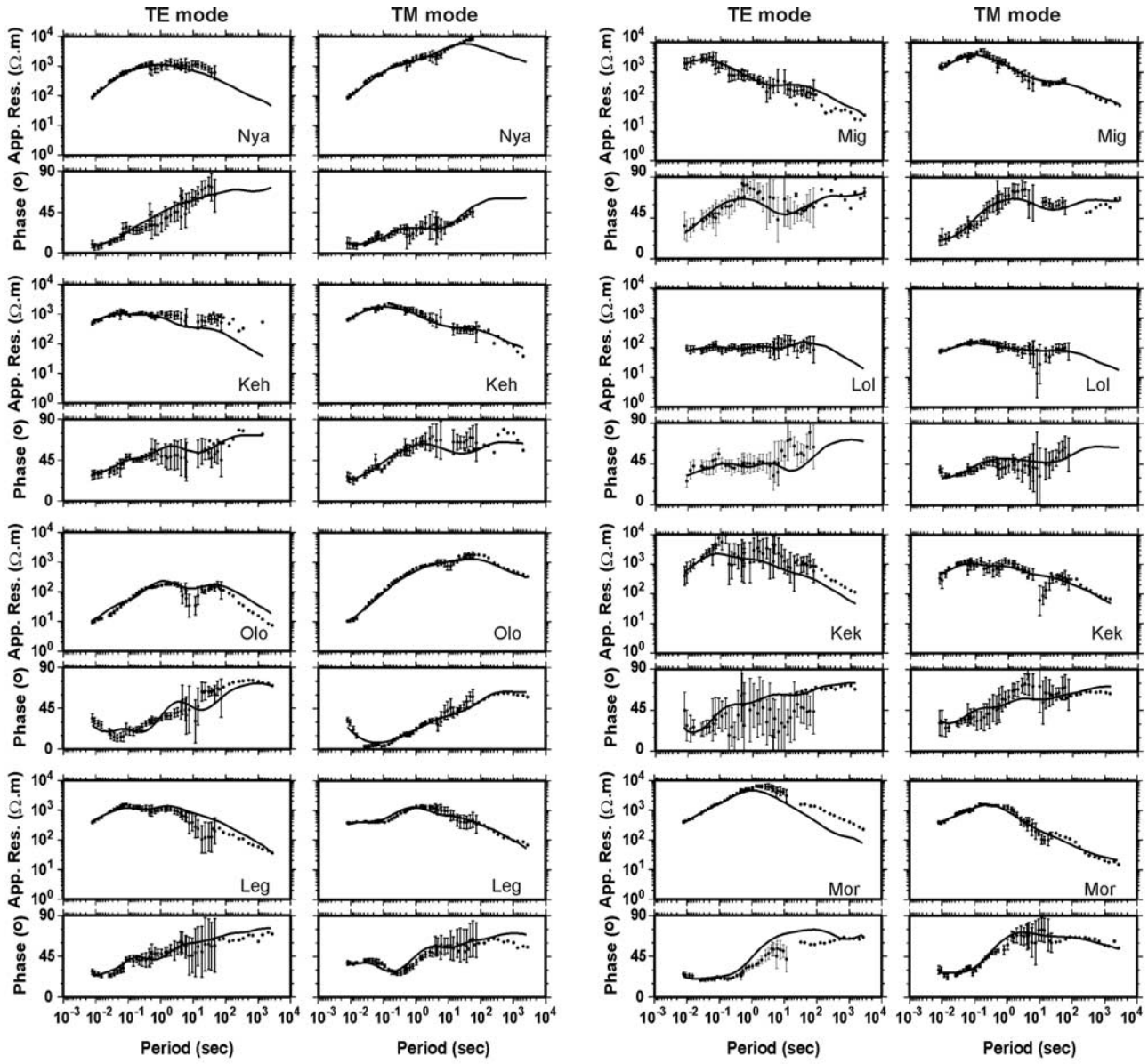

Figure 6a. Illustration of the fit between the measured data (shown with error bars) and the computed MT responses for the NYA-CHN minimum-structure model of Figure 5b (solid line) for the TE mode (left) and TM mode (right), showing stations NYA to MOR.

which is consistent with a 10 percent change of the normalized data misfit and can be determined using the formula [cf. *Meju*, 1994, equation (49)]

$$\mathbf{m}_{\mathrm{Qt}} = \left[(\mathbf{WA})^{\mathrm{T}}\mathbf{WA} + \varepsilon\mathbf{I}\right]^{-1}\left\{(\mathbf{WA})^{\mathrm{T}}\mathbf{d}^{*} + \varepsilon\mathbf{m}_{\mathrm{mnrms}} - \mu\mathbf{b})\right\} \quad (2)$$

where $\mu = \pm\{[\mathbf{Q}_{\mathrm{t}} - \mathbf{Q}_{\mathrm{nrms}}]/[\mathbf{b}^{\mathrm{T}}\,(\mathbf{WA})^{\mathrm{T}}\mathbf{WA} + \varepsilon\mathbf{I}]^{-1}\,\mathbf{b}]\}^{0.5}$, $\mathbf{W}$ is a diagonal matrix whose elements are the reciprocals of the actual field data errors, $\mathbf{A}$ is the matrix of partial derivatives determined using $\mathbf{m}_{\mathrm{nrms}}$, ε is a damping factor set equal to the value of τ used in generating $\mathbf{m}_{\mathrm{nrms}}$, $\mathbf{I}$ is the identity matrix, and $\mathbf{d}^{*} = [\mathbf{W}(\mathbf{d}^{\mathrm{cal}} - \mathbf{d}^{\mathrm{obs}}) + \mathbf{W}(\mathbf{Am}_{\mathrm{nrms}})]$. The vectors $\mathbf{d}^{\mathrm{obs}}$ and $\mathbf{d}^{\mathrm{cal}}$ are the MT field responses and those calculated by forward theory for $\mathbf{m}_{\mathrm{nrms}}$, respectively. There are two (plus and minus) solutions for μ and may be regarded as the upper and lower resistivity bounds for the specified $\mathbf{Q}_{\mathrm{t}}$ if the projection vector $\mathbf{b}$ is set up as a unit vector. We expect that poorly constrained parameters will yield a relatively wide range between the lower and upper solution bounds, but note that equation (2) implies that there is a compensating relationship between the model parameters [cf. *Meju and Hutton*, 1992].

[18] Owing to the size of the model (107 × 56 cells), we could not realistically extremize every resistivity cell but instead focused on site-by-site data constraints. Thus for each MT station, we first amalgamated the resistivity blocks from locations extending midway between adjacent stations in the horizontal direction and also grouped blocks of comparable resistivity (within 20%) in the vertical direction to form a column of blocks to be tested (Figure 7b). For consistent sampling, an additional column of blocks was

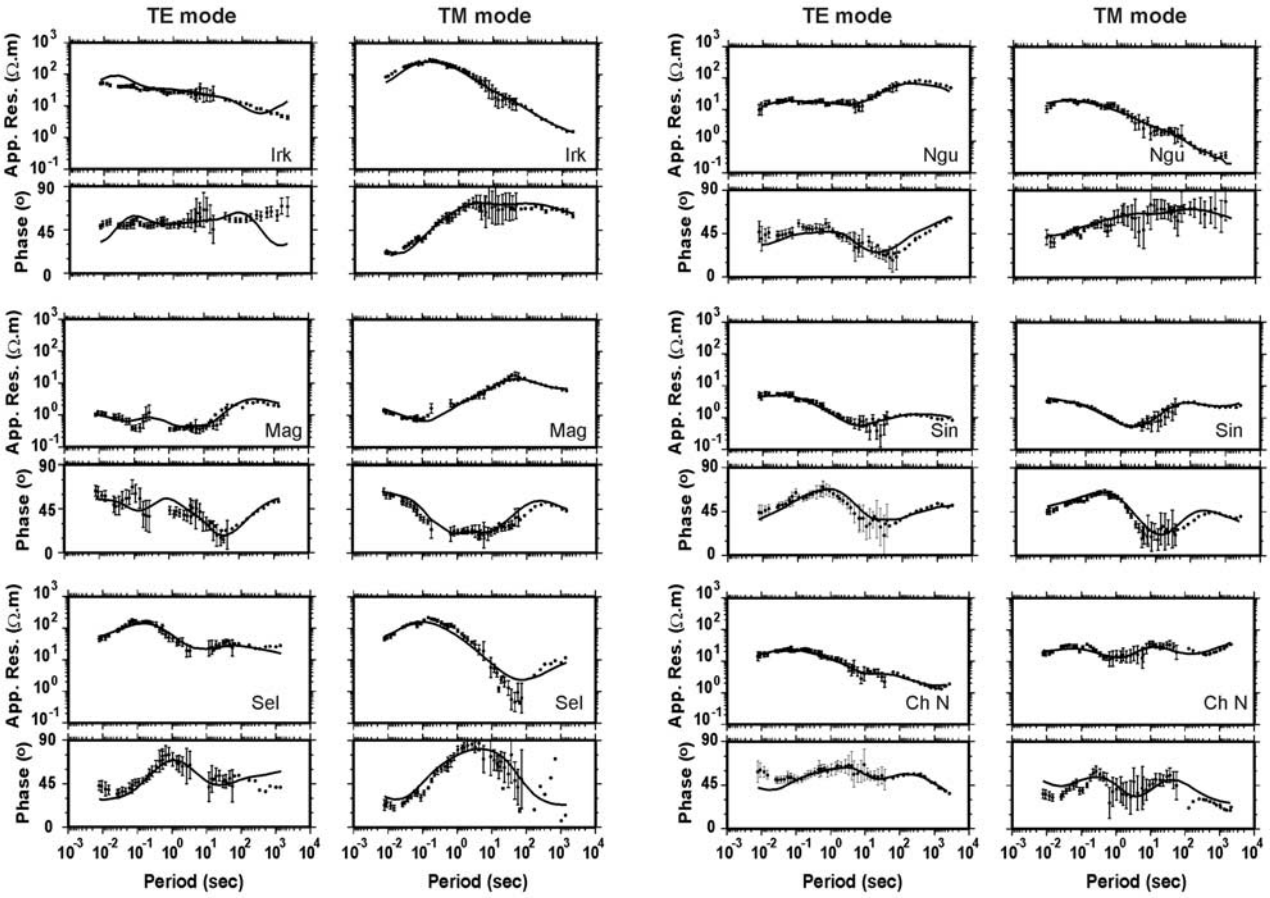

Figure 6b. Same as Figure 6a but for stations IRK to CHN. Note the large error bars (one standard deviation) in the dead band and the generally higher quality of the LMT data.

placed at the position of the aborted station (Kajiado) between SIN and SEL. We then set **b** equal to unity and calculated the parameter updates for $\mathbf{m}_{\mathrm{nrms}}$ that satisfy the threshold residual, $\mathbf{Q}_t$ and the compensating relationship between the model parameters embodied in equation (2). Considering the significant averaging involved in our approach, the resulting resistivity ranges may not be accurate but will suffice for a simple model appraisal. This analysis seems to suggest that structures deeper than 40 km are only sufficiently constrained by the field data outside the Rift Valley. In Figure 7b we present the estimated parameter ranges for the top 40 km of a model that satisfied equation (1) with a normalized residual error of 1.914 for the 2862 data points. It can be seen from the parameter ranges that many of the first-order electrical features maintain fairly narrow resistivity ranges relative to the corresponding block resistivities in the least-squares model of Figure 7a and are thus deemed to be justified by the field data. The same conclusion was also reached by *Sakkas* [1999]. What is perhaps unexpected in this simple analysis is the suggestion (Figure 7b) that the shallow crustal conductor G east of OLO and feature D near IRK may not be well-constrained in the blocky model and must therefore be interpreted with caution. It would also appear that a probably continuous, eastward-tapering or dipping resistive zone may be required in the deep crust (10–30 km) across the rift valley rather than the vertical through-going crustal conductive zone subcropping between NGU and MAG near the western rift margin as Figure 7a would suggest; however, an east-dipping crustal conductor (feature A) and a deeper vertical zone may exist at the eastern rift margin (profile position 255–270 km). In what follows, we will draw on the smooth inversion models which were not constructed using an assumed geological structure.

3.3. First-Order Features and Relationship With a Suggested Generic 3-D Model

[19] *Simpson*'s [2000] forward model comprises a N–S trending regional 2-D structure (shown in Figures 5a and 5b) with outcropping N–S trending 2-D rift half-grabens and 3-D profile-parallel deep crustal lineaments. Here, we compare the first-order features in our 2-D MT models with the regional 2-D structures in Simpson's generic model that was based on long period MV and MT phase data at only a few stations (MIG, OLO, LEG, MOR, IRK, NGU, MAG, SIN, and LUK) and an assumed background resistivity of 1000 Ωm for the region. The important first-order features of our 2-D MT inversion models are as follows.

[20] 1. The resistivity structure especially west of SIN consists principally of steeply-dipping alternating thick resistive and relatively thin conductive units. Since the sub-Moho resistor beneath OLO appears to be continuous

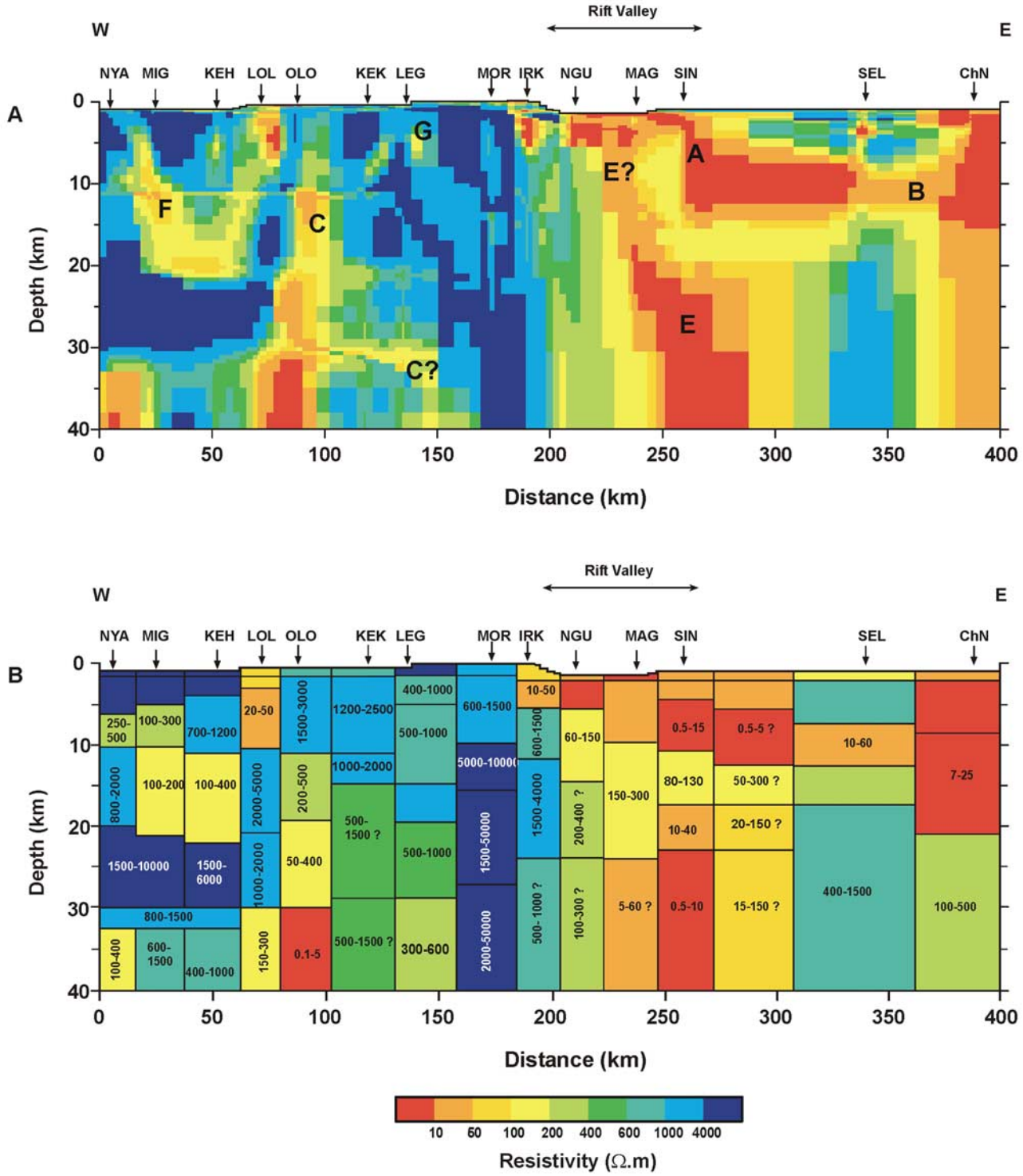

Figure 7. Illustration of 2-D resistivity model appraisal for the top 40 km of the NYA-CHN transect, showing (a) the optimal least squares model to be appraised and (b) the estimated resistivity range for each block that is consistent with a prescribed threshold misfit. Hot colors (yellow and red) indicate high conductivity and cool colors (blue and purple) indicate high resistivity.

with a near-surface body (feature H in Figure 5), these steep sequences may be crustal blocks.

[21] 2. Anomalous subhorizontal upper crustal conductors appear to be present in the top 10–15 km east of the rift margin (known to be highly sheared and affected by Quaternary volcanism) and at about 20 km depth in the NYA-MIG area where there was also Quaternary volcanism further north (see inset map in Figure 1).

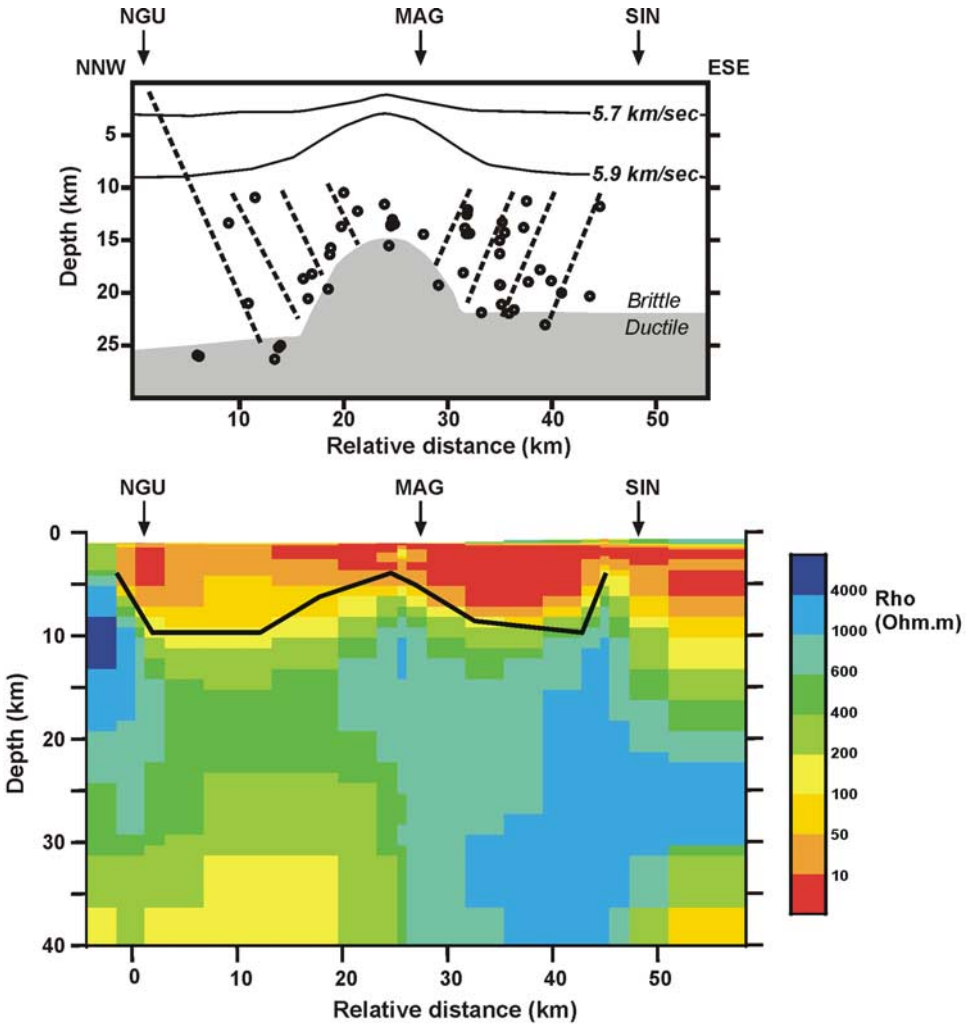

Figure 8. Comparison of crustal structure of the Kenya rift in Magadi area as determined by microseismic tomography and 2-D MT imaging along a coincident line. The top section is an interpretative model derived from combined 3-D local earthquake tomography and spatial distribution of hypocentres in the area [*Ibs-von Seht et al.*, 2001]. The circles are hypocenter depths. The dashed lines are assumed depth ranges of active faults and the solid lines give the velocity structure determined for the top 15 km of the crust [*Ibs-von Seht et al.*, 2001]. The lower section is extracted from Figure 5b and the w-shaped (double half-graben) structure of the rift proper is traced in black at the same depth as the 5.9 km/s refractor in the upper seismic model.

[22] 3. A prominent conductive zone dips eastwards from the near-surface at OLO to lower crustal depths (feature C). Feature C dips about 39° to the east in the top 23 km but appears to become steeper across the seismic Moho [*Birt et al.*, 1997]. In Figure 5b, it is possible that feature C becomes flat at about 70 km depth before bending upward to subcrop at the western rift margin but this structural continuity is not well-resolved by the data. Middle/lower crust 3-D conductive lineaments are proposed to extend from OLO to below both flanks of the rift but their depth and lateral positions are not constrained by the MV data [*Simpson*, 2000, p. 19,327]. If feature C does not extend significantly in our assumed strike direction, it would effectively constitute a buried elongate 3-D conductor and may be expected to cause a significant phase split in unrotated MT data [cf. *Sasaki and Meju*, 2006, Figure 5] as observed at OLO by *Simpson* [2000].

[23] 4. The E-dipping segments of conductors F, C, G, A, and B appear to be parallel (see Figures 5a and 5b) and spaced 40–60 km apart (the spacing being estimated perpendicular to a dip angle of 39°).

[24] 5. There is a 50 km wide zone with 4–8 km thick relatively conductive sequence beneath NGU to SIN in the Rift Valley. It is shallowest in the middle near station MAG, deepest in the west and most conductive in the east (Figure 8). It appears to be bordered to the east by a persistent E-dipping crustal conductor (feature A) coinciding with a major rift fault in Figure 1. The w-shape of its bottom in Figure 8 may suggest a double half-graben structure. In Simpson's model, there are two 3–5 km deep half-grabens in the rift valley and electrically conducting sediments are assumed to be deepest in the western half-graben.

[25] There are thus major differences between our 2-D inversion models and *Simpson*'s [2000] simple 3-D forward

model which did not include all the available MT data. The crustal structure of the Mara-Loita area was not clearly imaged in the 3-D study. The area of known basement shearing and Quaternary volcanism [*Bosworth*, 1987; *Macdonald*, 2003] is characterized by sub-horizontal upper crustal conductors in the 2-D models (features A and B) instead of the profile-parallel lineaments placed in the middle/lower crust underneath the rift in the model of *Simpson* [2000]. The 2-D smooth model generated from a 1000 Ωm half-space (Figure 5b) appears to be the closest to Simpson's interpretation of the regional structure. A pertinent question here is: how consistent are the 2-D MT images with the results from coincident seismic and gravity surveying and geological ground-truth?

4. Independent Model Appraisal: Consistency With Other Geophysical Results

4.1. Consistency Analysis of Shallow-Depth Resistivity Structure

[26] The MT model of Figure 5b suggests the rift valley as consisting of a conductive cover sequence of variable (4–8 km) thickness underlain by a resistive geoelectric basement. The W-shape of the interface between the conductive rift sequence and the basement (Figures 5b and 8) is in remarkable agreement with the borehole-constrained, shallow-depth, seismic velocity interpretation of the rift valley [see *Simiyu and Keller*, 2001, Figure 6]. Another coincident cross section from a 3-D microseismic study of the Lake Magadi area [*Ibs-von Seht et al.*, 2001, Figure 22] also produced a similar structure to that found between NGU and SIN in the top 10 km as shown in Figure 8. For this reason, we select the model shown in Figure 5b as our preferred model. The seismic model of *Birt et al.* [1997] suggests a near-layered crustal structure east of the rift and minor E-dipping disruption of the shallow crust in the vicinity of station CHN. Since this area exposes NW–SE ductile shears and thrust faults, any significant disruption of the relatively flat upper crustal structure could furnish constraints on the possible geometry and depth extent of these fracture systems. In Figures 5 and 7, two prominent subhorizontal shallow-depth conductors occur between SIN and CHN at about 5 to 15 km depth underneath a resistive cover. There is also an apparent change in the thickness of conductor B near station CHN in agreement with the coincident seismic model [*Birt et al.*, 1997]. Conductor B appears to be disrupted by a steeply dipping feature which may possibly be related to the NW–SE lineaments suggested on the surface. *Simiyu and Keller*'s [2001, Figure 13] integrated interpretation of the KRISP94 gravity data using deep seismic refraction constraints [*Birt et al.*, 1997] suggests an E-dipping contact in the top 15–18 km of the crust near the Oloololo Escarpment which is in accord with the electrical resistivity structure of the OLO area in the uppermost 10–20 km (Figure 5). As shown in Figure 9a, the location of this steep contact coincides with a previously predicted suture based on Bouguer gravity anomalies [*Tesha et al.*, 1997, Figure 6]. Another gravity low coincides with the projected outcrop zone of the sub-horizontal conductor A at the eastern rift margin (Figure 9a); the western edge of this conductor coincides spatially with a major rift fault (see Figure 1). It may be significant that the geoelectrically inferred 50 km width of the rift zone proper (Figure 8) is comparable to the 40–60 km separation between the E-dipping segments of prominent conductors (F, C, G, A, and B) and between the exposed NW–SE fracture systems east of the Rift Valley (Figure 1).

4.2. Consistency Analysis of Inferred Deep Resistivity Structure

[27] On the basis of the suggested Moho depth from a collocated seismic refraction survey [*Birt et al.*, 1997], the anomalous resistive blocks and the intervening conductor C in the Mara-Loita sector extend into the uppermost mantle. Using wide-angle seismic reflection data and assuming the roughly layered crustal structure derived by *Birt et al.* [1997], *Byrne et al.* [1997] infer the existence of two bands of discontinuous upper mantle reflectors (mimicked by discrete, very thin, high velocity layers at 51 and 63 km depths below the Oloololo Escarpment, the top reflector rising gently eastward to 43 km depth under the rift and then deepening to 50 km about 40 km further east). The bands of reflectors are superimposed on our preferred MT model for comparison in Figure 9b. The geometry of these sub-Moho reflectors is different from the steep structure suggested in the MT model but the geographical locations where the reflector continuity is broken appear to correlate spatially with the positions of conductors C, D, and E (Figures 5 and 9). Note that *Birt* [1996] identified an E-dipping reflector at 24.5 to 26 km depth near the Oloololo Escarpment which is coincident with the top of the anomalous resistive block beneath feature C (see Figure 9b). While our MT images (Figures 5 and 9b) differ significantly from the lithospheric structure suggested by these 2-D seismic models west of the rift valley, there are common features in the top 20 km east of the rift proper. The implied steep geoelectrical structure elsewhere is structurally consistent with the result of 3-D teleseismic tomography for the Chyulu Hills region [*Ritter and Kasper*, 1997]. An overlapping section of seismic P-velocity perturbations that runs eastwards from the SEL area for about 150 km (see Figures 2a and 2b) suggests the presence of E-dipping steep zones of alternating high- and low-velocities extending through the crust down to over 100 km depth [*Ritter and Kasper,* 1997, Figure 10]. It is significant that the spacing between the alternate zones of low- and high-velocity perturbations [see *Ritter and Kaspar, 1997*, Figure 10] is about 40–60 km which is in accord with our inference from the E-dipping conductors in Figures 5a and 5b. It may be no coincidence that the velocity anomalies are especially prominent in the 23 to 70 km depth range [*Ritter and Kasper*, 1997], which corresponds to the zone of steepest dip of geoelectrical features (see Figures 9b and 9c).

[28] The Bouguer gravity anomaly along the NYA-CHN transect [*Birt et al.*, 1997] is shown in Figure 9a for comparison with the resistivity pattern. Notice that the first 90 km of the MT profile (zone 1 in Figure 9a) is characterized by a gravity high; this correlates spatially with the area underlain by a persistent crustal conductor at 5–20 km depth (feature F) that has a bow-shape or basinal cross section. It also coincides spatially with an outcropping Archaean volcano-sedimentary (Migori greenstone) belt [e.g., *Ichang'l and MacLean*, 1991]. This is followed eastward by a zone of marked gravity low coincident with our profile positions 90 to 270 km (zone 2 in Figure 9a).

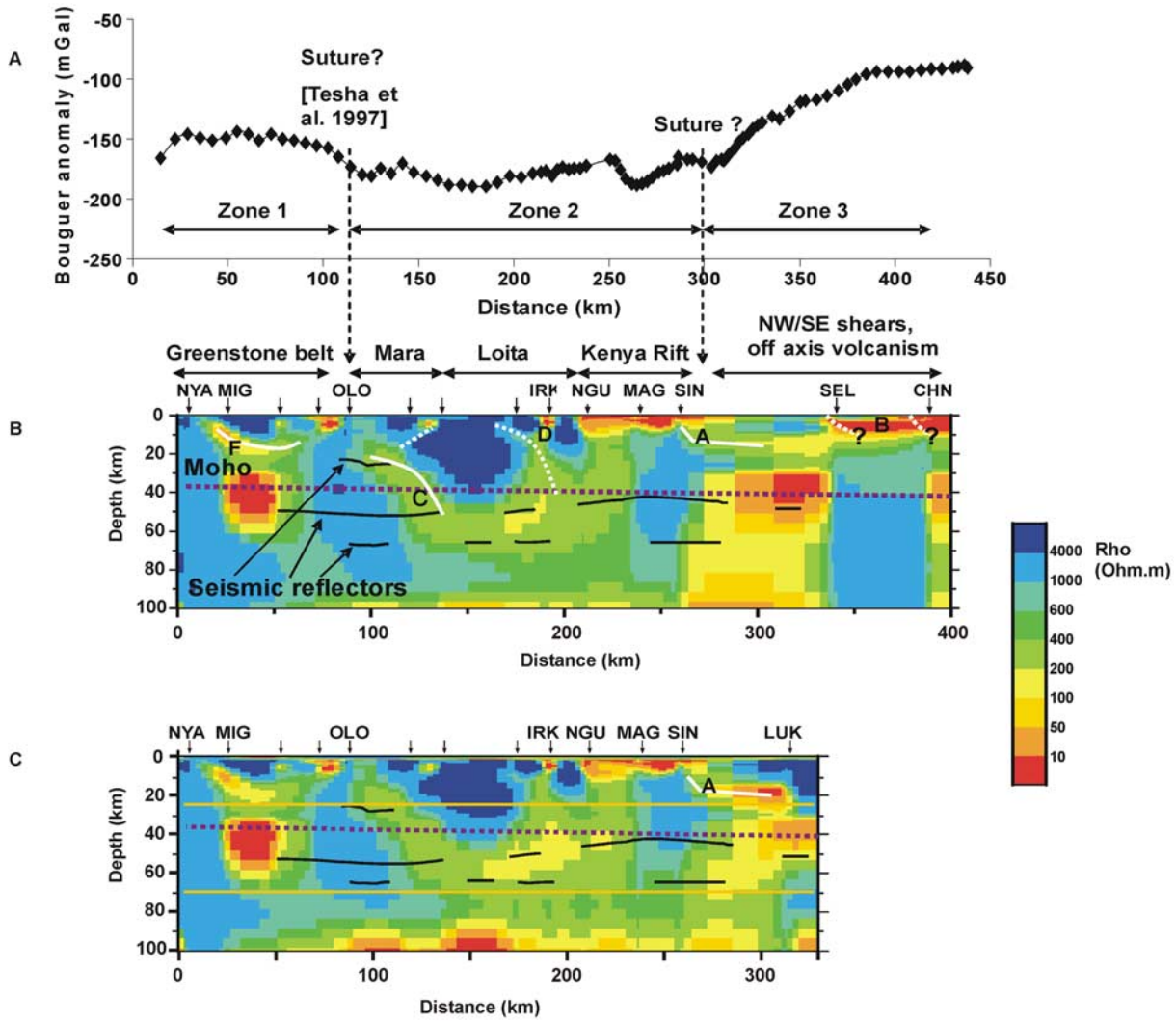

Figure 9. Comparison of MT, seismic and gravity signatures from collocated studies of the deep structure across southern Kenya. (a) Bouguer gravity anomaly along the survey line [*Birt et al.*, 1997]. Long vertical dashed lines indicate possible boundaries of distinct lithospheric blocks (zones 1–3) discussed in text. The position of a suture suggested by *Tesha et al.* [1997] is indicated. (b) MT model with superimposed (in black) sub-Moho wide-angle seismic reflectors [*Byrne et al.*, 1997] and a crustal reflector [*Birt*, 1996] for the NYA-CHN transect. The violet horizontal dotted line at 32–40 km depth shows the seismic Moho [*Birt et al.*, 1997]. Our inferred structural geometries in the crust and uppermost mantle (thick lines for principal and fine dots for subsidiary features) are shown in white. The principal geological features are indicated on top of the cross-section. (c) Resistivity model for a line incorporating station LUK to test further the existence of conductor A. The white line is a possible trace of conductor A. The golden lines at 23 and 70 km depths delimit a possible depth interval where structures are steepest [cf. *Ritter and Kasper*, 1997, Figure 10]. There is a 25 km offset between the starting points of the MT and gravity surveys.

The first part of this zone (position 90 to 195 km) includes the Loita area where there may be a buried Archaean crust and duplex-structures [*Mosley*, 1993]. Our resistivity models suggest the possible presence of a sequence of resistive and conductive units that is buckled or stacked up against feature C in the Loita area (cf. Figures 5, 7, and 9b) but it could also be a monolithic resistor disrupted by faulting. There is a small increase in the Bouguer gravity between positions 195 and 270 km, coinciding with the area delimited by features D and A, that spatially correlates with the Kenya rift. The two minima in the regional gravity field coincident with our inferred boundaries of zone 2 in Figure 9a have been suggested [*Tesha et al.*, 1997] as signatures representing the contributions from a suture-thickened crust (Neoproterozoic component) and the Kenya rift (Cenozoic component). Our MT model is consistent with the presence of relatively thickened upper crustal resistive blocks between OLO and IRK in zone 2. Further east (zone 3 in

Figure 9), the Bouguer anomaly profile rises very steeply while the MT models suggest the possible presence of subhorizontal crustal conductors underlain by an anomalous steep resistive block with flanking conductors. As indicated above, the MT results agree with the teleseismic tomographic results for this part of our transect [see *Ritter and Kasper*, 1997, Figure 10]. There is thus good correlation between our MT and other geophysical measurements on the NYA-CHN transect. We see these correspondences as permitting a geological discussion of our MT results but bearing in mind the band-limited nature of our data and the consequent limitation on model resolution.

5. Discussions

5.1. Is There a Link Between Resistivity Heterogeneity and Lithospheric Segmentation?

[29] Our electrical resistivity models (Figures 5, 7, and 9) suggest the presence of significant heterogeneities in the crust and presumed uppermost mantle across the study region. A striking feature is the predominance of a blocky structure rather than the nearly horizontally stratified structure suggested from other coincident 2-D surveys [e.g., *Birt et al.*, 1997; *Byrne et al.*, 1997] but this may also have been influenced by the wider station spacing used in our survey. The most prominent crustal marker zones are the bow-shaped craton conductor west of OLO (feature F), the steeply dipping conductor at OLO (feature C), and the subhorizontal conductors east of the main rift (features A and B). It is also possible that vertical conductive zones exist beneath stations IRK (where feature D also has an associated gravity signature), NGU and SIN, even though the analysis presented in Figure 7b suggests that they are not well resolved by the MT data. Notice that conductors F, C, and A in Figures 5 and 9b appear to be E-dipping in their western part but become subhorizontal and possibly continue further east with a westward (reversed?) dip suggesting some form of folding.

[30] The geometry of feature F below the outcropping resistive Archaean crust probably suggests a folded or buckled crustal domain. This is consistent with geological observations of major folding and thrusting in this Archaean sector [e.g., *Pinna et al.*, 2000]. Feature F appears to be separated from feature C by a thin steep resistor (feature H) that connects to the anomalous resistive block beneath feature C in the OLO area. Is the resistive block directly above feature C a dismembered Archaean crust? *Mosley* [1993] predicts that an Archaean crust is buried by duplex-structures in the Loita area. The MT models suggest the possible presence of alternating resistive and conductive buckled units above feature C in the Mara-Loita sector (position 90 to 195 km) which may thus be part of a fold and thrust belt. The region from position 195 to 270 km appears to be an extensively faulted crustal upwarp (near-vertical conductors are apparent at IRK, NGU, and SIN). East of the rift margin (zone 3 in Figure 9), the upper crustal structure is strikingly subhorizontal but this could be a consequence of the sparse data sampling or the obliquity of our survey line to the regional structural trend. We noted that inverting the MT data for a subset of stations (KEK to LUK) lying parallel to the profile of *Rooney and Hutton* [1977] (see Figure 1) or for stations NYA to LUK (Figure 9c) did not eliminate the need for conductor A, which appears as a prominent 38° E-dipping feature that flattens at 20 km depth and possibly suggests that a major thrust-like feature separates zone 2 from the LUK area of outcropping Mozambique belt (Table 1).

[31] It would thus appear that the evinced regionalisation of resistivity structures from west to east probably reflects some form of lithospheric-scale structural segmentation (or buckling) and compositional zoning, with the main zones being delimited by conductive features (Figure 9b). These zones appear to coincide spatially with positions of change in geological patterns on the surface, and their principal electrical conductors coincide with positions of low Bouguer gravity anomalies (see Figure 9a) and low seismic velocities [e.g., *Ritter and Kasper*, 1997; *Tesha et al.*, 1997; *Simiyu and Keller*, 2001]. We therefore propose that there is a possible link between the imaged deep resistivity heterogeneity and surface-mapped deformation both in the craton and the MOB of southern Kenya. The rifting and magmatism in the study region are probably localized by preexisting lithospheric heterogeneity as also suggested by past studies based on different geophysical measurements [e.g., *Smith and Mosley*, 1993; *Birt et al.*, 1997] but we illuminate the steep structure of this possible thrust and fold belt and opine that the lithosphere may be severely buckled in the region. It is significant that a proposed division of the basement geology of this region into three NW–SE striking blocks or domains comprising the Archaean Tanzanian craton, an intermediate zone of reworked Archaean rocks and the Proterozoic Mozambique belt [*Smith and Mosley*, 1993] is in good agreement with our inferred crustal zonation in southern Kenya (Figure 9). The 100-km-wide zone of reworked Archaean observed in northwest Kenya and which played a central role in the proposition of *Smith and Mosley* [1993] appears to correlate with our zone 2.

5.2. Electrical Conductors: Partial Melt, Sutures, or Reactivated Shear Zones?

[32] What is the nature or role of the evinced conductive zones in the different crustal compartments? The superficial conductor on the rift floor may correspond to the infill of sediments and volcanic debris impregnated with hot saline fluids. Conductor B may be a permeable fluid migration pathway impregnated with hot or salty volcanogenic fluids since it is restricted to an area of intensely sheared basement [*Smith and Mosley*, 1993] and recent volcanism [*Bosworth*, 1987]. Note that if conductor B is cut by the steep shallow-depth conductors suggested to be related to the outcropping NW–SE lineaments (Figure 9b), then it must be a preexisting feature in the basement rather than a product of recent off-axis magmatism. Another plausible explanation, drawing on what is emerging from MT studies of other active rift systems [e.g., *Oskooi et al.*, 2005], is that it could be a clay-mineralized geochemical alteration zone above a differently altered, electrically resistive preexisting basement or juvenile crust. The deep conductive zones at the rift margins and the ill-constrained flat conductor (feature E) beneath the inferred resistive block across the rift valley (Figures 5 and 9) may thus be part of an alteration halo and not a partial melt. Can this explain the zone of microseismicity confined at 12–25 km depth [*Ibs-von Seht et al.*, 2001] in the resistive crust within the rift zone (Figure 8)? It is noteworthy that *Simiyu and Keller* [2001] suggest that the low velocities and

densities observed under the western flank of the rift probably represent reworked Archaean Tanzania craton.

[33] Conductor F spatially underlies the Archaean Migori greenstone belt stretching E–W for 80 km [*Ichang'l and MacLean*, 1991]. If this conductor were an Archaean volcano-sedimentary layer, we may invoke metallic sulphide mineralization and/or graphitization as a possible electrical conduction mechanism. However, while the coincident Bouguer gravity anomaly profile (Figure 9a) would suggest the presence of excess mass in this locality, the absence of anomalous high-velocity layer corresponding to feature F in the collocated seismic velocity model [*Birt et al.*,1997] is inconsistent with large-scale massive sulphide mineralization. Instead, a reflective midcrustal boundary at 17 km depth [*Birt et al.*, 1997] coincides with the base of feature F, which may thus be a low-velocity or low-density feature such as a sag basin buried by overthrust Archaean basement or volcanic arc fragment [cf. *Solon et al.*, 2005]. It is perhaps significant that a small fault-bounded basin is suggested near OLO (Figure 1) while the Nyanza rift zone (NRZ in Figure 1) occurs further north from station NYA. However, our preferred explanation is that the principal conductive markers are probably reactivated Precambrian shear zones or deformed mechanically weak layers between rigid crystalline blocks that may have served for preferential transport or fluid focusing in the region. Our reasoning here is based on two important observations. First, they appear to have coincident low resistivity and Bouguer gravity anomalies (Figure 9a) and low seismic P-velocities [e.g., *Ritter and Kasper*, 1997]. Second, the localities of known Holocene volcanoes in the region (see Figure 1 and inset map) roughly coincide with the positions where anomalous steeply dipping sub-Moho conductors are well-developed on the NYA-CHN transect, specifically near NYA, MAG-SIN, and the Chyulu Hills.

[34] Note that some problems are left unresolved in this study. While conductor C may have separated different continental blocks, it is possible that postsuturing events have modified the region to the extent that it is difficult to clarify whether it is the true suture zone between the Tanzania craton and the MOB [e.g., *Tesha et al.*, 1997] and not one of several possible exposures of the same units repeated by large-scale periodic folding and thrusting. It is also unclear how the Neoproterozoic ophiolite and granulite trains seen on the surface further north of our study area (Figure 1) are related to the proposed basement heterogeneity. Is the entire lithosphere buckled by horizontal compression related to Precambrian collision or later far-field tectonics (e.g., owing to mid-Atlantic or mid-Indian Ocean ridge-push forces [*Zoback*, 1992]) such that these ophiolites and granulites are repeated at upwarped crustal sections? Is the Kenya rift a buckle-induced feature given that it appears to be located on what might be a crustal upward (Figures 5 and 9)? How is lithospheric buckling related to the observed Cenozoic volcanism? Is it the case that buckling lifted the borders of inverted preexisting basins forming antiforms whose uplifted margins became rapidly eroded facilitating the exhumation of deeper rocks (such as the granulites found near the margins of zones 1 and 2 (Figure 1) [*Shackleton*, 1986; *Smith and Mosley*, 1993]) leading ultimately to adiabatic decompression and fusion? Answers to these questions will have to await another integrated, preferably 3-D, field experiment.

6. Conclusion

[35] We have investigated the structure of the crust and upper mantle in southern Kenya using 2-D magnetotelluric data imaging. The models reconstructed using different inversion approaches show many common features. A simple model appraisal suggests that most of these common model features are consistent with the field data. Comparisons of the resistivity models and other geophysical results from collocated surveys show that the models are robust and also provide new information. The MT models suggest lithospheric-scale resistivity heterogeneity and possible lateral structural and/or compositional zoning from west to east in our study area. The electrical crust appears to consist of alternate east-dipping resistive and conductive blocks rather than continuous horizontally stratified layers. There is a major E-dipping conductor at Oloolololo but the true suture zone between the Tanzania craton and the Proterozoic Mozambique orogenic belt may lie east of the Rift Valley. The areas between the Oloolololo and Irkimba escarpments and east of the rift valley are characterized by anomalously thick crust while the Kenya Rift valley and the exposed Archaean sector between Migori and Oloolololo appear to have relatively thinner electrically resistive crust. We have shown that there appears to be a strong link between deep electrical heterogeneity and major geological features seen on the surface.

[36] **Acknowledgments.** We are grateful to F. Simpson, M. Eisel, V. Haak, and M.A. Khan for field support in the Kenya experiment sponsored by the European Union Human mobility programme and to Randy Mackie for the 2-D inversion codes. We thank the NERC Geophysical Equipment Facility in Edinburgh for a loan of the SPAM Mk2b field equipment and University of Leicester for the TEM equipment used in this study. We gratefully acknowledge the constructive comments by J.C. Mutter, Stephen Park, Martyn Unsworth, and an anonymous reviewer which helped improve the clarity of this paper.

References

Agarwal, A. K., H. E. Poll, and J. T. Weaver (1993), One- and two-dimensional inversion of magnetotelluric data in continental regions, *Phys. Earth Planet. Inter.*, *81*, 155–176.

Bahr, K. (1991), Geological noise in magnetotelluric data: A classification of distortion types, *Phys. Earth Planet. Inter.*, *66*, 24–38.

Bahr, K., M. Bantin, C. Jantos, E. Schneider, and W. Storz (2000), Electrical anisotropy from electromagnetic array data: Implications for the conduction mechanism and for distortion at long periods, *Phys. Earth Planet. Inter.*, *119*, 237–257.

Bai, D., and M. A. Meju (2003), Deep structure of the Longlin-Ruili fault zone underneath Ruili basin near the eastern Himalayan syntaxis: Insights from magnetotelluric imaging, *Tectonophysics*, *364*, 135–146.

Banks, R. J., and D. Beamish (1979), Melting in the crust and upper mantle beneath the Kenya rift: Evidence from geomagnetic depth sounding experiments, *J. Geol. Soc. London*, *136*, 225–233.

Beamish, D. (1977), The mapping of induced currents around the Kenya Rift: A comparison of techniques, *Geophys. J.R. Astron. Soc.*, *50*, 311–332.

Berhe, S. M. (1990), Ophiolites in northeast and East Africa: Implications for Proterozoic crustal growth, *J. Geol. Soc. London*, *147*, 41–57.

Birt, C. (1996), Geophysical investigation of active continental rifting in southern Kenya, Ph.D. thesis, 214 pp., Univ. of Leicester, U. K.

Birt, C., P. K. H. Maguire, M. A. Khan, H. Thybo, G. R. Keller, and J. Patel (1997), The influence of pre-existing structures on the evolution of the southern Kenya Rift Valley—Evidence from seismic and gravity studies, *Tectonophysics*, *278*, 211–242.

Bosworth, W. (1987), Off-axis volcanism in the Gregory Rift, East Africa: Implications for the models of continental rifting, *Geology*, *15*, 397–400.

Byrne, G. F., A. W. B. Jacob, J. Mechie, and E. Dindi (1997), Seismic structure of the upper mantle beneath the southern Kenya Rift from wide angle data, *Tectonophysics*, *278*, 243–260.

Chen, L., J. R. Booker, A. G. Jones, N. Wu, M. J. Unsworth, W. Wei, and H. Tan (1996), Electrical conductive crust in southern Tibet from INDEPTH magnetotelluric surveying, *Science*, *274*, 1694–1695.

Constable, S. C., R. L. Parker, and C. G. Constable (1987), Occam's inversion: A practical algorithm for generating smooth models from electromagnetic sounding data, *Geophysics*, *52*, 289–300.

Groom, R. W., and R. C. Bailey (1989), Decomposition of the magnetotelluric impedance tensor in the presence of local three-dimensional galvanic distortion, *J. Geophys. Res.*, *94*, 1913–1925.

Ibs-von Seht, M., S. Blumenstein, R. Wagner, D. Hollnack, and J. Wohlenberg (2001), Seismicity, seismotectonics and crustal structure of the southern Kenya Rift—New data from Lake Magadi area, *Geophys. J. Int.*, *146*, 439–453.

Ichang'l, D. W., and W. H. MacLean (1991), The Archaen volcanic facies in the Migori segment, Nyanza greenstone belt, Kenya: Stratigraphy, geochemistry and mineralization, *J. Afr. Earth Sci.*, *13*, 277–290.

Ledo, J., A. G. Jones, and I. J. Ferguson (2002), Electromagnetic images of a strike-slip fault: The Tintina fault—Northern Canada, *Geophys. Res. Lett.*, *29*(8), 1225, doi:10.1029/2001GL013408.

Maboko, M. A. H. (2000), Nd and Sr isotopic investigation of the Archaean-Proterozoic boundary in northeastern Tanzania: Constraints on the nature of Neoproterozoic tectonism in the Mozambique Belt, *Precambrian Res.*, *102*, 87–98.

Macdonald, R. (2003), Magmatism of the Kenya Rift Valley: A review, *Trans. R. Soc. Edinburgh Earth Sci.*, *93*, 239–253.

Mackie, R., S. Rieven, and W. Rodi (1997), Users manual and software documentation for two-dimensional inversion of magnetotelluric data, report, Earth Resour. Lab. Mass. Inst. of Technol., Cambridge, 12 July .

Meju, M. A. (1994), Biased estimation: A simple framework for parameter estimation and uncertainty analysis with prior data, *Geophys. J. Int.*, *119*, 521–528.

Meju, M. A. (1996), Joint inversion of TEM and distorted MT soundings: Some effective practical considerations, *Geophysics*, *61*, 56–65.

Meju, M. A., and V. R. S. Hutton (1992), Iterative most-squares inversion: Application to magnetotelluric data, *Geophys. J. Int.*, *108*, 758–766.

Meju, M. A., S. L. Fontes, M. F. B. Oliveira, J. P. R. Lima, E. U. Ulugergerli, and A. A. Carrasquilla (1999), Regional aquifer mapping using combined VES-TEM-AMT/EMAP methods in the semi-arid eastern margin of Parnaiba Basin, Brazil, *Geophysics*, *64*, 337–356.

Meju, M. A., L. A. Gallardo, and A. Mohamed (2003), Evidence for correlation of electrical resistivity and seismic velocity in heterogeneous near-surface materials, *Geophys. Res. Lett.*, *30*(7), 1373, doi:10.1029/2002GL016048.

Mohamed, A. K., M. A. Meju, and S. L. Fontes (2002), Deep structure of the northeastern margin of Parnaiba basin, Brazil, from magnetotelluric imaging, *Geophys. Prospect.*, *50*, 589–602.

Moller, A., K. Mezger, and V. Schenk (1998), Crustal age domains and the evolution of the continental crust in Mozambique belt of Tanzania, *J. Petrol.*, *39*, 749–783.

Mosley, P. N. (1993), Geological evolution of the late Proterozoic "Mozambique belt" of Kenya, *Tectonophysics*, *221*, 223–250.

Nyamai, C. M., N. Opiyo-Akech, S. J. Gaciri, and H. Fujimaki (1999), Geochemistry and tectonomagmatic affinities of the Mozambique belt intrusive rocks in Matuu-Masinga area, central Kenya, *Gondwana Res.*, *2*, 387–399.

Nyamai, C. M., E. M. Mathu, N. Opiyo-Akech, and E. Wallbrecher (2003), A reappraisal of the geology, geochemistry, structures and tectonics of the Mozambique belt in Kenya, east of the rift system, *Afr. J. Sci. Technol.*, *4*, 51–71.

Nyblade, A. A., and H. N. Pollack (1992), A gravity model for the lithosphere in western Kenya and northeastern Tanzania, *Tectonophysics*, *212*, 257–267.

Oskooi, B., L. B. Pedersen, M. Smirnov, K. Arnason, H. Eysteinsson, A. Manzela, and DGP Working Group (2005), The deep geothermal structure of the Mid-Atlantic Ridge deduced from MT data in SW Iceland, *Phys. Earth Planet. Inter.*, *150*, 183–195.

Pinna, P., A. Cocherie, D. Thieblemont, and P. Jezequel (2000), The Kisii Group of western Kenya: An end-Archaean (2.53 Ga) late orogenic volcano sedimentary sequence, *J. Afr. Earth Sci.*, *30*, 79–97.

Ritter, J. R. R., and T. Kasper (1997), A tomography study of the Chyulu Hills, *Kenya, Tectonophysics*, *278*, 149–169.

Rodi, W., and R. L. Mackie (2001), Nonlinear conjugate gradients algorithm for 2D magnetotelluric inversions, *Geophysics*, *66*, 174–187.

Rooney, D., and V. R. S. Hutton (1977), A magnetotelluric and magnetovariational study of the Gregory rift valley, Kenya, *Geophys. J. R. Astron. Soc.*, *51*, 91–119.

Sakkas, V. A. (1999), Combined transient electromagnetic and magnetotelluric study of the southern Kenya Rift Valley, Ph.D. thesis, 250 pp., Univ. of Leicester, U. K.

Sakkas, V., M. A. Meju, M. A. Khan, V. Haak, and F. Simpson (2002), Magnetotelluric images of the crustal structure of Chyulu Hills volcanic field, Kenya, *Tectonophysics*, *346*, 169–185.

Sasaki, Y., and M. A. Meju (2006), Three-dimensional joint inversion for magnetotelluric resistivity and static shift distributions in complex media, *J. Geophys. Res.*, *111*, B05101, doi:10.1029/2005JB004009.

Shackleton, R. M. (1986), Precambrian collision tectonics in Africa, *Spec. Publ. Geol. Soc. London*, *19*, 329–349.

Shackleton, R. M. (1993), Tectonics of the lower crust: A view from the Usambara Mountains, NE Tanzania, *J. Struct. Geol.*, *15*, 663–671.

Shackleton, R. M. (1996), The final collision zone between east and west Gondwana: Where is it?, *J. Afr. Earth Sci.*, *23*, 271–287.

Simiyu, S., and G. R. Keller (1997), An integrated analysis of lithospheric structure across the East African plateau based on gravity anomalies and recent seismic studies, *Tectonophysics*, *278*, 291–313.

Simiyu, S., and G. R. Keller (2001), An integrated geophysical analysis of the upper crust of the southern Kenyan rift, *Geophys. J. Int.*, *147*, 543–561.

Simpson, F. (2000), A three-dimensional electromagnetic model of southern Kenya Rift: Departure from two-dimensionality as a consequence of a rotating stress field, *J. Geophys. Res.*, *105*, 19,321–19,334.

Simpson, F. L., V. Haak, M. A. Khan, V. Sakkas, and M. A. Meju (1997), The KRISP-94 magnetotelluric survey of early 1995: First results, *Tectonophysics*, *278*, 261–272.

Smith, M. (1994), Stratigraphic and structural constraints on mechanisms of active rifting in the Gregory Rift, Kenya, *Tectonophysics*, *236*, 3–22.

Smith, M., and P. Mosley (1993), Crustal heterogeneity and basement influence on the development of the Kenya Rift, East Africa, *Tectonics*, *12*, 591–606.

Solon, K. D., et al. (2005), Structure of the crust in the vicinity of the Banggong-Nujiang suture in central Tibet from INDEPTH magnetotelluric data, *J. Geophys. Res.*, *110*, B10102, doi:10.1029/2003JB002405.

Soyer, W., and M. Unsworth (2006), Deep electrical structure of the northern Cascadia (British Columbia, Canada) subduction zone: Implications for the distribution of fluids, *Geology*, *34*, 53–54.

Stern, R. J. (1994), Arc assembly and continental collision in the Neoproterozoic East African Orogen: Implication for the consolidation of Gondwana, *Annu. Rev. Earth Planet. Sci.*, *22*, 319–351.

Sternberg, B. K., J. C. Washburne, and L. Pellerin (1988), Correction for the static shift in the magnetotellurics using transient electromagnetic soundings, *Geophysics*, *53*, 1459–1468.

Tesha, A. L., A. A. Nyblade, G. R. Keller, and D. I. Doser (1997), Rift localization in suture-thickened crust: Evidence from Bouguer gravity anomalies in northeastern Tanzania, East Africa, *Tectonophysics*, *278*, 315–328.

Unsworth, M., W. Wenbo, A. G. Jones, S. Li, P. Bedrosian, J. Booker, J. Sheng, D. Ming, and T. Handong (2004), Crustal and upper mantle structure of northern Tibet imaged with magnetotelluric data, *J. Geophys. Res.*, *109*, B02403, doi:10.1029/2002JB002305.

Wannamaker, P. E., G. W. Hohmann, and S. H. Ward (1984), Magnetotelluric responses of three-dimensional bodies in layered earths, *Geophysics*, *49*, 1517–1533.

Zoback, M. L. (1992), First- and second-order patterns of stress in the lithosphere: The World Stress Map Project, *J. Geophys. Res.*, *97*, 11,703–11,728.

M. A. Meju, Department of Environmental Science, Lancaster University, Lancaster LA1 4YQ, UK. (m.meju@lancaster.ac.uk)

V. Sakkas, Department of Geothermy and Geophysics, National and Kapodistrian University of Athens, Panepistimiopolis, Ilissia Athens GR-15784, Greece. (vsakkas@geol.uoa.gr)